Final Technical Report
June 2008

# Shear-wave Velocity Determination for Metropolitan St. Louis Focal Mechanism

USGS Grant 05HQGR0046

Robert B. Herrmann and David J. Crossley
Department of Earth and Atmospheric Sciences
Saint Louis University
3642 Lindell Boulevard, O'Neil Hall
St. Louis, MO 63108

TEL: 314-977-3120, FAX 314-977-3117, Email rbh@eas.slu.edu

Key words: Shallow shear-wave velocity

Final Technical Report
June 2008

# Shear-wave Velocity Determination for Metropolitan St. Louis Focal Mechanism

USGS Grant 05HQGR0046

Robert B. Herrmann and David J. Crossley
Department of Earth and Atmospheric Sciences
Saint Louis University
3642 Lindell Boulevard, O'Neil Hall
St. Louis, MO 63108

TEL: 314-977-3120, FAX 314-977-3117, Email rbh@eas.slu.edu

Key words: Shallow shear-wave velocity

## Abstract

This effort focused on the determination of shallow S-wave velocity structure at various sites in the metropolitan St. Louis area using a 24-channel digital seismograph. Separate reversed profile experiments were performed using vertical and transversely oriented seismometers with vertical and transverse hammer sources, respectively, spaced every 3 meters with hammer source offsets of 1, 2 and 3 meters to yield a 72 meter spread for each profile. The vertical source and vertical sensor combination is used to determine the P-wave first arrivals and Rayleigh wave dispersion while the horizontal source and transverse sensor combination is used to determine the SH-wave first arrivals and Love wave dispersion. Preliminary models are presented evaluate the combined P- and S-wave velocity depth structure at the sites.

## 1. Introduction

The determination of shallow S-wave velocities at a site is essential for defining the Vs30 used site characterization for earthquake ground motion. There are many methods in use for defining the S-wave velocity structure sufficiently for the specification of this number. In-situ measurements can be performed using a seismo-piezocone and up-hole techniques. Surface measurement techniques include refraction, reflection and surface-wave techniques with the latter being either active or passive. Another indirect measure entails the use of a three-component sensor at the surface to estimate the frequency dependent H/Z ratio.

Each technique has its own strengths and weaknesses, which are summarized in Table 1. The importance of this statement can been seen in a comparison of shallow S-wave velocity structure on a test site on the Saint Louis University campus. The U. S. Geological Survey group (Jack Odum, Bill Stephenson, Rob Williams and others) performed several experiments (Fig 1.1). The seismic data were used to make refraction/reflection and Remi (a technique to determine surface-wave dispersion using a linear array and ambient noise) estimates of the S-wave velocity structure. At a subsequent time, the University of Missouri – Rolla group (currently called the Missouri University of Science and Technology) used a similar deployment of only vertical sensors to determine the shallow S-wave

velocity structure using the Kansas Geological Survey MASW (multi-channel analysis of Surface Waves) procedure.

**Table 1. Comparison of techniques for determining shallow seismic velocity**

| Technique | Strengths | Weaknesses |
|---|---|---|
| Refraction | • Simple observations – first arrival times<br>• Simple inversion procedure | • Difficulty in picking first arrival<br>• Difficulty in making a robust estimate of the halfspace velocity because of small move-out over spread length and too short of a spread |
| Reflection | • Definition of layering | • Cannot determine velocity of halfspace<br>• Must be able to see reflections |
| Surface-wave | • Easily observed | • Determination of dispersion requires significant processing<br>• Depth resolution related to range of observed frequencies<br>• Little resolution of boundaries |
| H/R | • Simple field procedure<br>• Simple signal processing | • Interpretation is complicated |

Fig. 1.1. View of St. Louis University test site. R. Williams of the USGS (left with back to camera). This display shows the beam used for the horizontal source as well as the spread of vertical and transverse geophones deployed for the experiment.

Figure 1.2 compares the velocity models obtained using the different techniques. The velocities in the halfspace are a continuation of the velocity of the deepest point given for each technique. Since no other information is know *a priori,* this is just one possible distribution at depth. All models agree well in the S-wave velocity estimate in the upper 10 meters, but differ significantly beneath that depth. The

observation of a refracted arrival with a velocity of 1.2 km/s forces the estimate of about 10 meters for the soil-rock interface at the site, a value that agrees with known borehole information in the region. Because of the smooth nature of the surface-wave dispersion and because of the lack of sensitivity of the surface-wave inversion kernels to one specific depth, it is no surprise that the surface-wave data cannot discern the layer boundary.

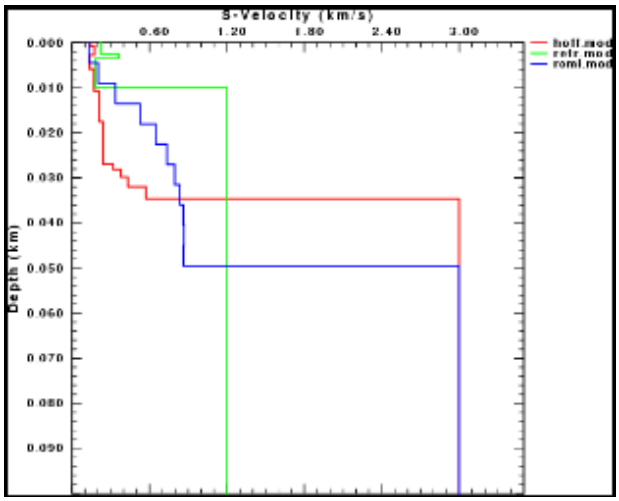


Fig. 1.2. Comparison of S-wave velocity profiles using different techniques: MASW (red) courtesy D. Hoffman of MWR; refraction (green) USGS; REMI (blue) USGS.

The other problem with the surface-wave technique is related to the limited frequency range for which dispersion is observed. One rule-of-thumb is that the surface-wave depth resolution is on the order of 1/10 or 1/20 of the spread length (here 8 and 4 meters respectively for a nominal 80 meter spread), or that the depth is on the order of 1/3 of the longest wavelength (5 meters for a period of 0.1 sec and a phase velocity of 150 m/s). If a significant feature is identified on the dispersion curve, e.g., a steep slope of the dispersion at a given frequency, the dependence of the point as the layer thickness changes is such that the quantity Vs/fH is constant, where Vs is the S-wave velocity, f is the frequency and H is the layer thickness. Thus if the velocities are fixed, the given feature will appear at a higher frequency as the layer thickness decreases. On our experiments in the St. Louis area with a 70 meter spread and a nominal 10 meter layer thickness, we found that the phase velocity dispersion curve begins to be affected by the deeper structure at frequencies less than 10 Hz, a frequency range for which we have little information. Thus we conclude that we must use a longer spread and correspondingly more energetic source in order to use the dispersion to get information if the soil-rock interface is deeper than 10 m.

As mentioned the S-wave velocity structure is required to be able to estimate the value of Vs(30). Using the structures given in Fig. 1.2, we would have values of 202 m/s (UMR MASW), 311 m/s (USGS Remi) and 448 m/s (USGS refraction ) for the models from each of the techniques listed above. Although these numbers might yield site classifications of D or C, an even more interesting effect is on the frequency dependent site amplification. Figure 1.3 compares the 1-D vertically propagating SH-amplification using the codes from David Boore's SMSIM package:

(http://quake.wr.usgs.gov/~boore/software_online.htm).

Focusing either on the either the solid or dashed curves, one sees significant differences in the frequency dependent site response which are due to the fact that the sediment – rock boundary is shallow and/or the fact the velocity is poorly resolved at depth.

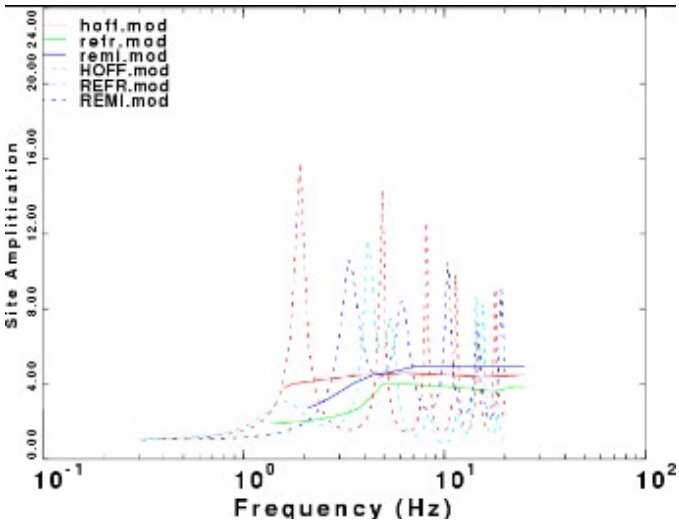


Fig 1.3. Comparison of site response for each of the velocity models shown in Fig. 1.2: UMR-MASW (red), USGS-refraction (green) and USGS Remi (blue). The solid curves are the one-quarter wavelength estimates of site amplification and the dashed curves show the vertically propagating SH-response using D. Boores program *rattle* (http://quake.wr.usgs.gov/~boore/software_online.htm ).

We suggest that in the St. Louis area, Vs(30) is not adequate to describe the frequency dependent site response and further suggest that it must be augmented with the thickness of the low velocity sediments.

**2. Methodology**

The field procedure we used follows that of the USGS. A 24 channel system of 4.5 Hz geophones was used for this study. They were generally placed in three-meter spacing, with multiple shot points to provide greater resolution when studying the refractions. Shot points are located one and two meters off each end of the array and on each end of the array to yield an effective spread of 72 meters with a 1 meter separation between geophones. The shot points were then moved to the other end of the spread to provide data for a reversed profile. the spread could not be made much longer than 72 meters because of the fixed length of the geophone string and because of the difficulty of creating an energetic enough hammer source to provide the signal to propagate over such a large distance.

In the field, a vertical source combined with 4.5 Hz vertical geophones was used to obtain P-wave first arrivals and Rayleigh-wave phase velocities, while a horizontal hammer source was used with 4.5 Hz horizontal sensors oriented transverse to the line for the determination of SH-wave first arrivals and Love-wave dispersion.

Since we did not have an inversion program to invert the dispersion and first-arrival data sets, we determine the velocity structure using the first-arrival data and then test that model against the surface-wave phase velocities.

After acquiring the field data, each trace in the SEG2 file is converted to the Sac format using the program *seg2tosac* written by J. Mejia. The conversion process places the shot and receiver locations as well as the source-receiver distance into the Sac header for use by the analysis programs. We organize the data sets by SITE and then by P or SH/Shot Records, and then process the traces.

As an example of the processing, we consider the data collection at Bellefontaine Park West, collected June 28,2005. All shots used a 0.5 ms sampling with a 1024 ms record length (2048 points). At this site the following data files were collected:

1. S wave experiments

| Shot # | filename | shot position | repetitions |
|---|---|---|---|
| 1 | 1146.dat | 0.0 N end | 13 |
| 2 | 1147.dat | 0.0 S end | 15 |
| 3 | 1148.dat | 1.0 N end | 15 |
| 4 | 1149.dat | 1.0 S end | 15 |
| 5 | 1150.dat | 2.0 N end | 15 |
| 6 | 1151.dat | 2.0 S end | 13 |
| 7 | 1152.dat | 73.0 N end | 13 |
| 8 | 1153.dat | 73.0 S end | 13 |
| 9 | 1154.dat | 72.0 N end | 13 |
| 10 | 1155.dat | 72.0 S end | 13 |
| 11 | 1156.dat | 71.0 N end | 12 |
| 12 | 1157.dat | 71.0 S end | 12 |

2. P wave experiments

Included are 6 additional shot positions on the East and West extensions of the array.

| Shot # | filename | shot position | repetitions |
|---|---|---|---|
| 1 | 1158.dat | 101.0 | 13 |
| 2 | 1159.dat | 100.0 | 13 |
| 3 | 1160.dat | 99.0 | 13 |
| 4 | 1161.dat | 73.0 | 12 |
| 5 | 1162.dat | 72.0 | 13 shot line problems |
| 6 | 1163.dat | 71.0 | 10 |
| 7 | 1164.dat | 0.0 | 12 |
| 8 | 1165.dat | 1.0 | 12 |
| 9 | 1166.dat | 2.0 | 10 |
| 10 | 1167.dat | -30.0 | 8 |
| 11 | 1168.dat | -29.0 | 9 |
| 12 | 1169.dat | -28.0 | 11 |

3. Noise tests

Sampling 2 ms, record length 32 768 ms, P phones.

| Test # | filename |
|---|---|
| 1 | 1170.dat |
| 2 | 1171.dat |
| 3 | 1172.dat |
| 4 | 1173.dat |
| 5 | 1174.dat |
| 6 | 1175.dat |
| 7 | 1176.dat |
| 8 | 1177.dat |

```
9       1178.dat
10      1179.dat
```

We processed the data in the following fashion. First we created directories corresponding to each data file created by the recorder, e.g., 1169. The 1169.dat was then converted into Sac files using the program seg2tosac. We then used gsac to view the traces and to make picks of the first arrivals. For the SH arrivals on the transverse components, the traces were bandpass filtered between 40 and 80 Hz, while the vertical traces were bandpass filtered between 80 and 150 Hz. First arrival picks were selected using the data from shots 1148, 1149 and 1150 for SH and 1164, 1165 and 1166 for P. Strong reflections stood out on the SH profile while none were seen in the P-SV profile.

The first arrival time information obtained is summarized by the equations:

```
S: Refr t0 0.000003 p 6.172431 (sec/km) Vel 0.162011 (km/sec) Refractor 1
S: Refr t0 0.168790 p 0.544079 (sec/km) Vel 1.837969 (km/sec) Refractor 2

S: Refl t0 0.144137 p 5.758160(sec/km) Vrms 0.173667(km/sec) Reflector 1 Multiple 1
S: Refl t0 0.312168 p 6.157072(sec/km) Vrms 0.162415(km/sec) Reflector 1 Multiple 2
S: Refl t0 0.438229 p 6.174935(sec/km) Vrms 0.161945(km/sec) Reflector 1 Multiple 3

P: Refr t0 -0.000445 p 3.106521 (sec/km) Vel 0.321904 (km/sec) Refractor 1
P: Refr t0  0.030275 p 0.405935 (sec/km) Vel 2.463450 (km/sec) Refractor 2
P: Refr t0  0.036726 p 0.207117 (sec/km) Vel 4.828198 (km/sec) Refractor 3
```

Using these observations and simple refraction analysis we would have a refraction velocity model

| H(km) | Vp(km/s) | Vs(km/s) |
|---|---|---|
| 0.0049 | 0.321 | 0.162 |
| 0.0089 | 2.463 | 0.162 |
| - | 4.838 | 1.837 |

Interestingly the analysis of the independent P- and SH-wave data sets yields the same depth the the high velocity interface of about 13.8 meters. The P- and S-wave velocity in the top layer have a ratio typical of rock or dry soil. In the second layer the much larger ratio can be attributed to an increase in the P-wave velocity beneath the ground water table. The ratio in the halfspace is too great for typical rock.

The SH reflections can be interpreted in terms of a single layer of velocity 0.162 km/s and thickness of 0.012 km, which is near the value derived from the refraction analysis.

Although the first arrival analysis provides a simple velocity model, there are problems with the technique. First, it is difficult to read the beginning of the first arrival precisely, especially since the polarity of the direct and refracted waves can differ. The arrivals at short distance, which control the very shallowest part of the model, are difficult to read because the sensors detect movement due to swinging the hammer. At large distances, the near-zero slope makes the velocity determination very sensitive to small changes in the arrival time pick. For typical field experiments, it is difficult to get data at distances greater than 100 meters because of site specific limitations on the sensor deployment

and because the low energy signal is difficult to see at these large distances.

The data sets did have good recordings of surface waves – Rayleigh on the verticals and Love on the transverse components. Using the Computer Programs in Seismology program *do_pom* (Herrmann, 2003), phase velocity dispersion can be estimated using all traces for the Love- and Rayleigh-wave studies. We then used other programs in the package to make forward predictions based on the refraction model derived above. The predicted dispersion fit neither at the high or lower frequencies. As a test, we modified the layer thicknesses of the velocity model, and then used the program *surf96* to redefine the velocity model. The resultant model is

| H(km) | Vp(km/s) | Vs(km/s) | Density (gm/cm^3) |
|---|---|---|---|
| 0.0010 | 0.421 | 0.173 | 1.69 |
| 0.0010 | 0.306 | 0.126 | 1.58 |
| 0.0029 | 0.308 | 0.154 | 1.65 |
| 0.0044 | 1.746 | 0.149 | 1.64 |
| 0.0044 | 2.535 | 0.215 | 1.77 |
| - | 4.828 | 2.238 | 2.46 |

As a test of this model, Figures 2.1 and 2.2 compare the observed and predicted Love- and Rayleigh-wave dispersion while Figures 2.3 and 2.4 compare the P- and SH-wave first arrival times.

The model as constructed fits all data sets well. However the Figure 2.5 shows that the model does not fit the observed reflections at large offset.

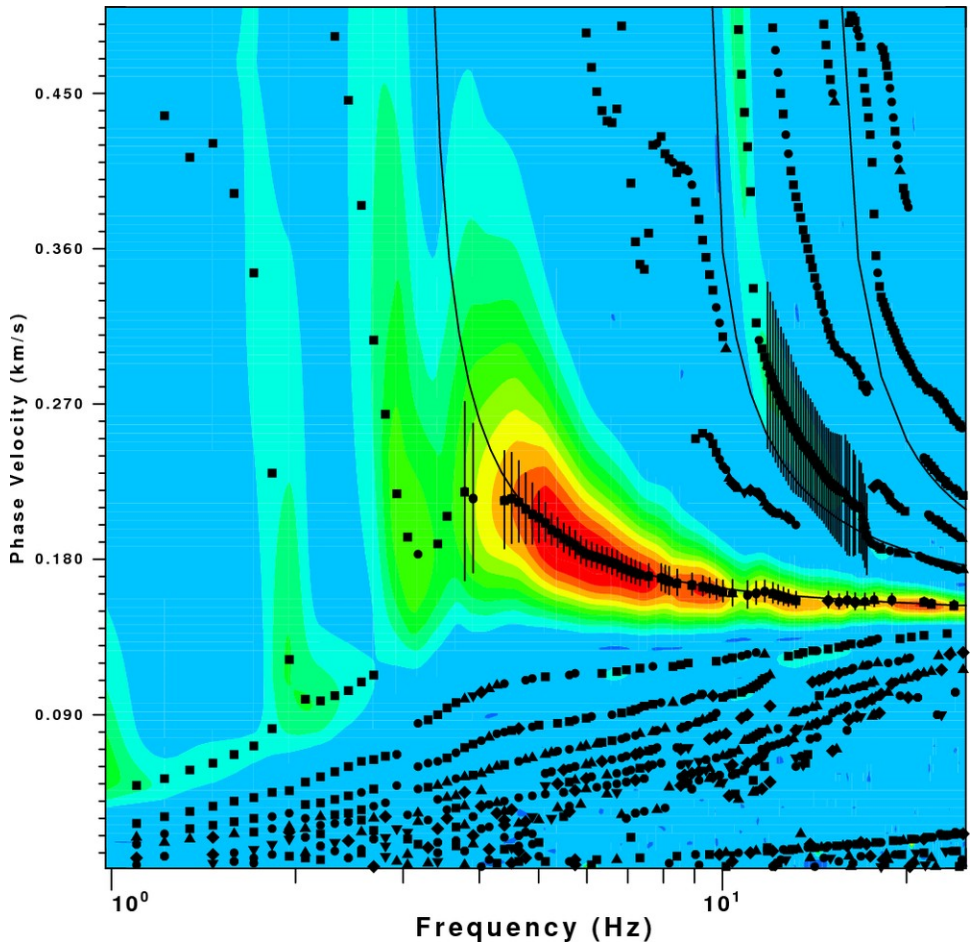


Fig. 2.1. Observed and predicted Love-wave phase-velocity dispersion. The colored contours represent the value of the p_omega(f,c) function, with red being a well defined value. The various points on the plot indicate either other modes or the aliasing inherent in the process. The points with error bars are the phase velocities selected from the contour. The predictions of the fundamental and 1st and 2nd higher modes are given by the solid black lines.

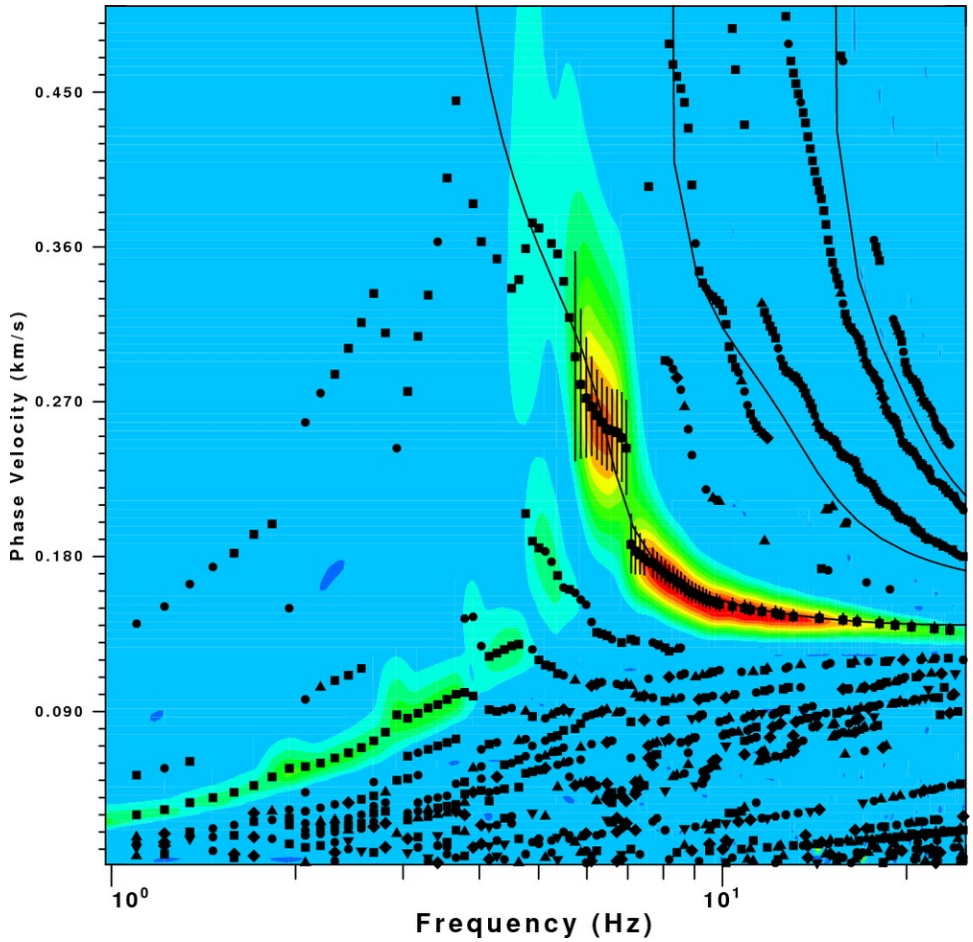


Fig. 2.2. Observed and predicted Rayleigh-wave phase-velocity dispersion.

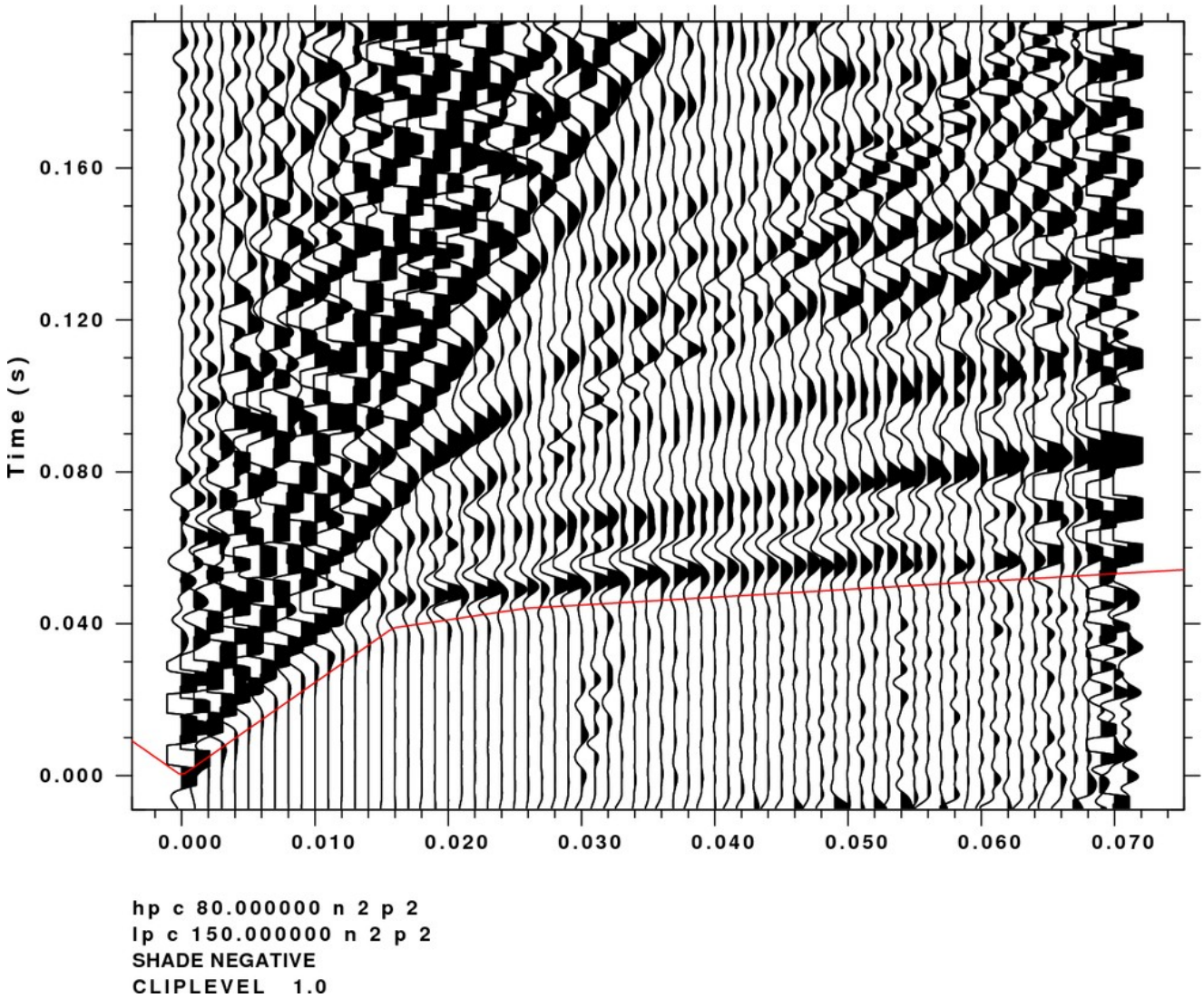


Fig. 2.3. Observed and predicted P-wave first arrivals. The plot annotation indicates the gsac commands used for bandpass filtering the traces. The red curve is the first arrival time prediction based on the model. There may be some evidence of reflection, perhaps from a depth of 30 meters or a P-S conversion.

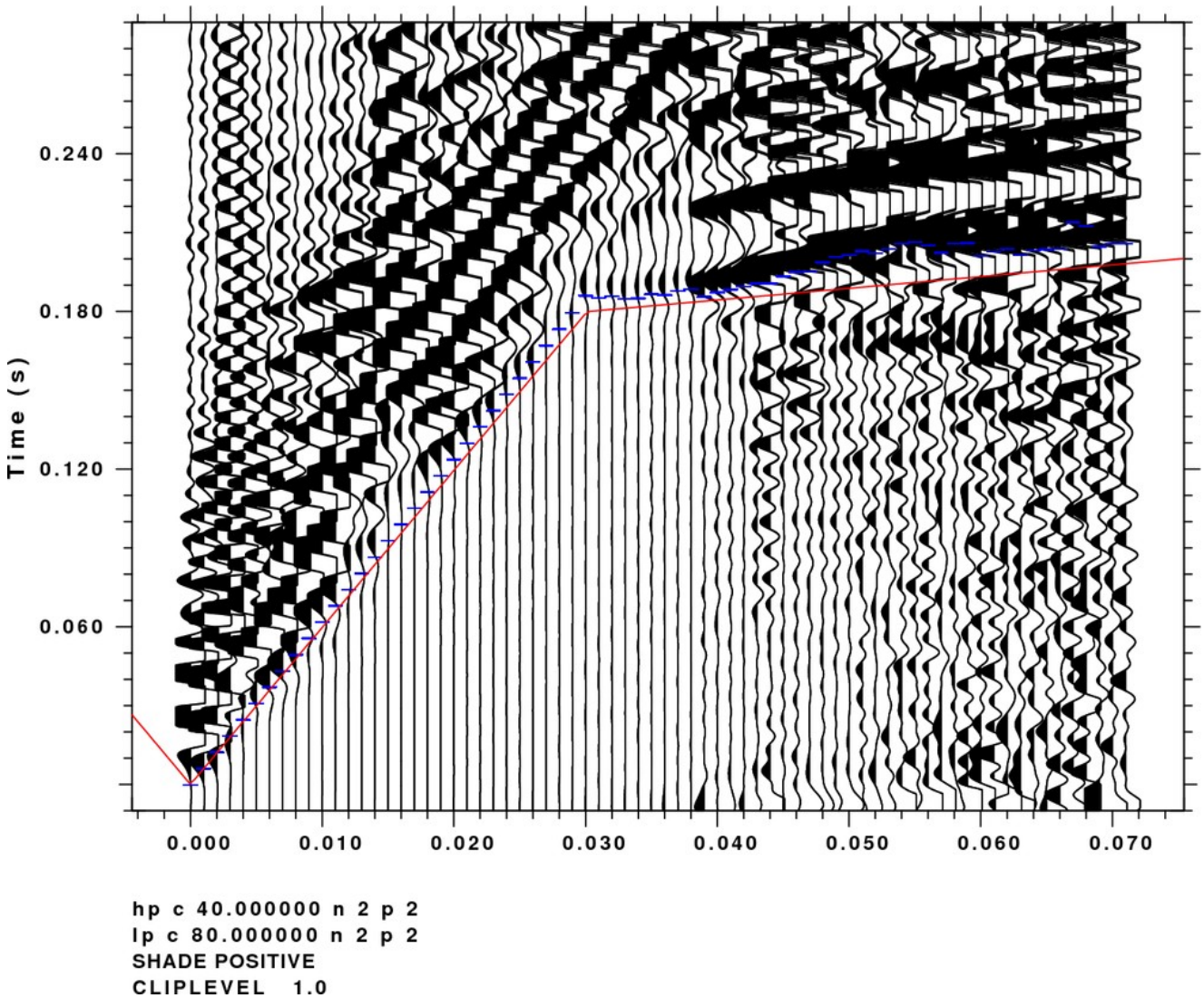


Fig. 2.4. Observed and predicted SH-wave first arrivals. The plot annotation indicates the gsac commands used for bandpass filtering the traces. The blue tics are first arrival picks which the red curve shows the model prediction of the first arrival time.

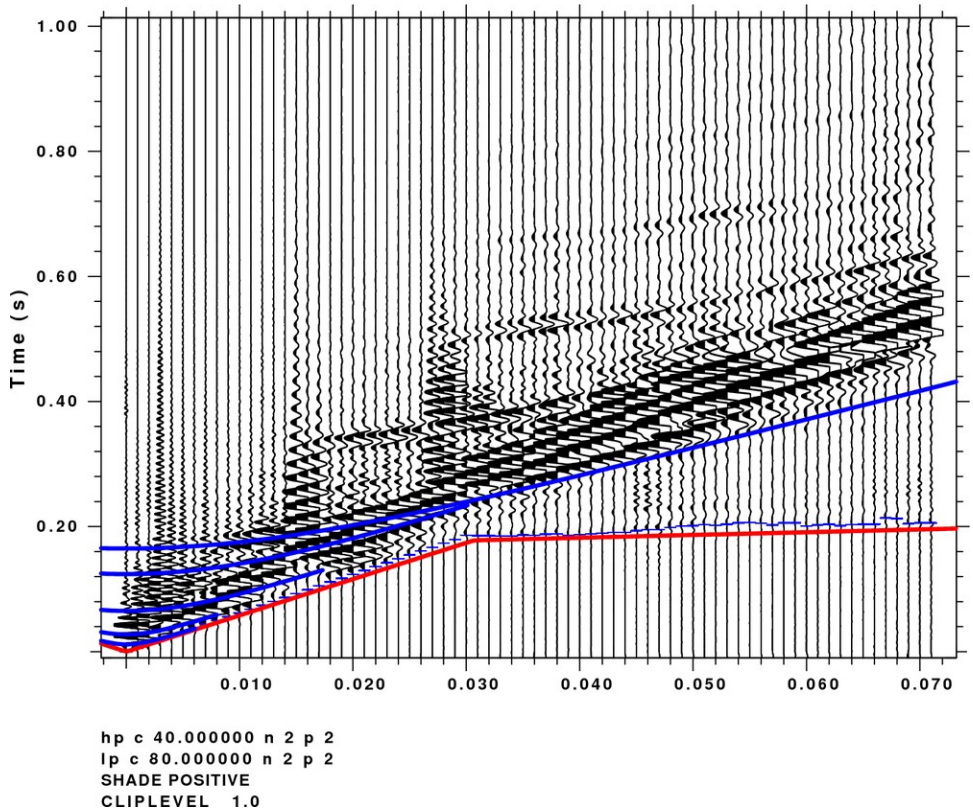


Fig. 2.5. Comparison of model predictions for SH first arrival (red) and first reflection from each interface in the layer (blue). Note that the amplitude will be related to the impedance contrast of the reflecting layer; thus only the top blue curve would be observed. Note that the model does not fit the observed reflection/direct arrival at large offset.

The conclusion of this exercise is that we were able to estimate a layers P- and S-wave velocity model for this site with very little effort. The real task would be to automate the many manual inversion steps into a simple, documented set of procedures that accounts for the errors in the observations. Perhaps the best way is to ignore the refraction intercept and velocity coming from the *refr* command in the program *gsac* and to use the first arrival times directly. The use of the reflection data would be even more difficult since the surface-waves will be sensitive to gradients within the layers, whereas the reflections are sensitive to both the average velocity structure and the impedance contrast across the layer boundaries. The inversion program should be designed to provide an estimate in the confidence in the model as a function of depth, perhaps by providing a suite of models derived from a Monte Carlo approach.

## 3. Field Investigations

The field investigations performed are summarized in the following table.

**S-wave Velocity Field Program Summer 2005**

| Date | Site | Files | Comments |
|---|---|---|---|
| 20050308 | SLU test – soccer field<br>38.6361N, 90.2364W | 1001-1010 | Done by Bob Herrmann and students |
| 20050603 | St. Charles Community College<br>38.759N, 90.643W | 1011-1019 | Most S files are noisy, due to phones? P wave files 1016, 1017 and 1018 are OK |
| 20050607 | SLU test Macelwane Hall/ Laclede Avenue | 1020-1023 | P-wave only, reversed and shot 10 m off ends |
| 20050614 | SLU test – soccer field<br>38.6361N, 90.2364W | 1027-1044 | wet and very mushy, poor S-wave |
| 20050615 | Meramec River, Georgia Tech Site<br>38.4588N, 90.3504W | 1045-1052 | wet site along road |
| 20050623 | Fairground Park, Granite City quad<br>38.6642N, 90.2183W | 1054-1077<br>1078-1083 | S wave completed<br>P wave aborted due to trigger problems<br>continued next day put in same directory |
| 20050624 | O'Fallon Park, Granite City Quad | 1084-1112 | Gently sloping ground, noisy (grass cutting) |
| 20050627 | Bellefontaine Park, Granite City Quad<br>38.6801N, 90.2304W | 1113-1145 | open area west side of park |
| 20050628 | Bellefontaine West, Granite City Quad (described in Section 2)<br>38.7411N, 90.2706W | 1146-1179 | Site below baseball field |
| 20050630 | Riverview Park, Granite City Quad<br>38.7433N, 90.1993W | 1180-1237 | Full set of S and P with off-end shots both ends. Shots had to be repeated next day due to trigger problems |
| 20050706 | Jefferson Community College<br>38.2575N, 90.5585W | 1238-1276 | Close to ANSS site |
| 20050707 | SIU Edwardsville<br>38.7846N, 89.9865W | 1277-1314 | Close to ANSS site |
| 20050708 | Edwardsville Athletic Club<br>38.7873N, 90.0124W | 1315-1370 | Just off SIUE on river plain |

At each site the following field procedures were followed.

Geometry:

A 24 channel system of 4.5 Hz geophones was used for this study. They were generally placed in three meter spacing, with multiple shot points to provide greater resolution when studying the refractions. Shot points are located one and two meters off each end of the array and on each end of the array.

Data acquisition:

Sampling interval of 0.5 ms and a record length of 1024 ms.

P-Wave & S-Wave Survey Techniques:

Ten to thirteen shots were stacked for each shot point for both P and S waves. Autostack was used most often. However, for sites with a higher noise level, preview mode was selected to delete noisy shots from the stack. Each S-Wave shot point has two sets of shots, which are located at either end of the S-Wave source, perpendicular to the array.

Noise Tests:

Noise tests were completed at each site. Ten noise tests were completed with the P phones, each lasting roughly 30 seconds. Then, a three-component noise test was completed. This was done by placing one S phone facing north, one S phone facing east, and one P phone in very close proximity. Also, the same three component assembly was constructed with 2 Hz geophones and included in the noise test.

### 3.1. Bellefontaine Park West

The analysis of this data set was presented in detail in Section 2. The velocity model derived is

| H(KM) | VP(KM/S) | VS(KM/S) | RHO(GM/CC) |
|---|---|---|---|
| 0.0010 | 0.421 | 0.173 | 1.69 |
| 0.0010 | 0.306 | 0.126 | 1.58 |
| 0.0029 | 0.308 | 0.154 | 1.65 |
| 0.0044 | 1.746 | 0.149 | 1.64 |
| 0.0044 | 2.535 | 0.215 | 1.77 |
| - | 4.828 | 2.238 | 2.46 |

### 3.2. Riverview Park

The P-wave first arrival data were not sufficient to determine the velocity of the halfspace because of the noise. The SH data set was used to define the layer boundaries. The P-velocity in the halfspace was set based on the S-wave velocity. The results of the processing leads to the following velocity model:

| H(KM) | VP(KM/S) | VS(KM/S) | RHO(GM/CC) |
|---|---|---|---|
| 0.0038 | 0.2988 | 0.1030 | 1.5102 |
| 0.0038 | 0.4689 | 0.1615 | 1.6665 |
| 0.0039 | 1.8702 | 0.6234 | 2.1358 |
| 0.0039 | 1.8557 | 0.6187 | 2.1332 |
| 0.0039 | 1.8415 | 0.6139 | 2.1305 |
| 0.0039 | 1.8277 | 0.6091 | 2.1278 |
| 0.0200 | 5.0074 | 3.1047 | 2.5014 |
| 0.0000 | 5.0000 | 3.1000 | 2.5000 |

The following figures compare the observed and predicted phase velocity dispersion and compare the raw data with the predicted first motions.

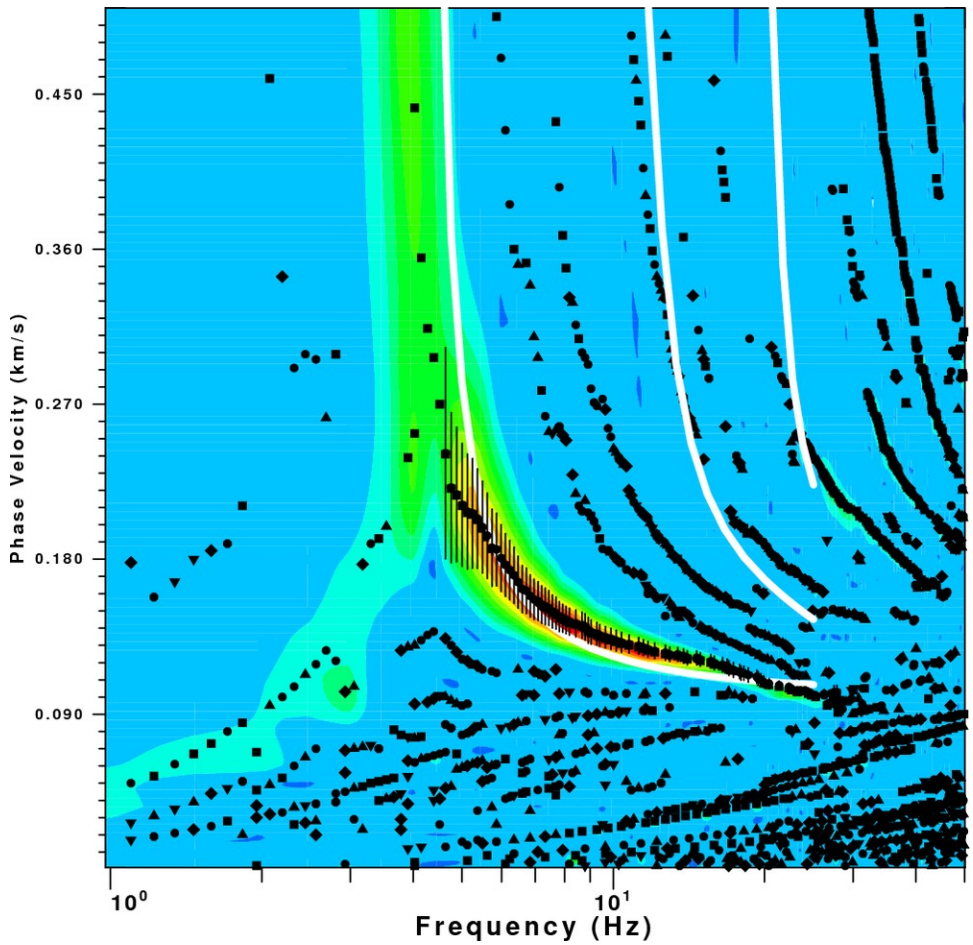


Fig. 3.1. Observed and predicted Love-wave phase-velocity dispersion for the Riverview site. The colored contours represent the value of the p_omega(f,c) function, with red being a well defined value. The various points on the plot indicate either other modes or the aliasing inherent in the process. The points with error bars are the phase velocities selected from the contour. The predictions of the fundamental and 1st and 2nd higher modes are given by the solid white curves.

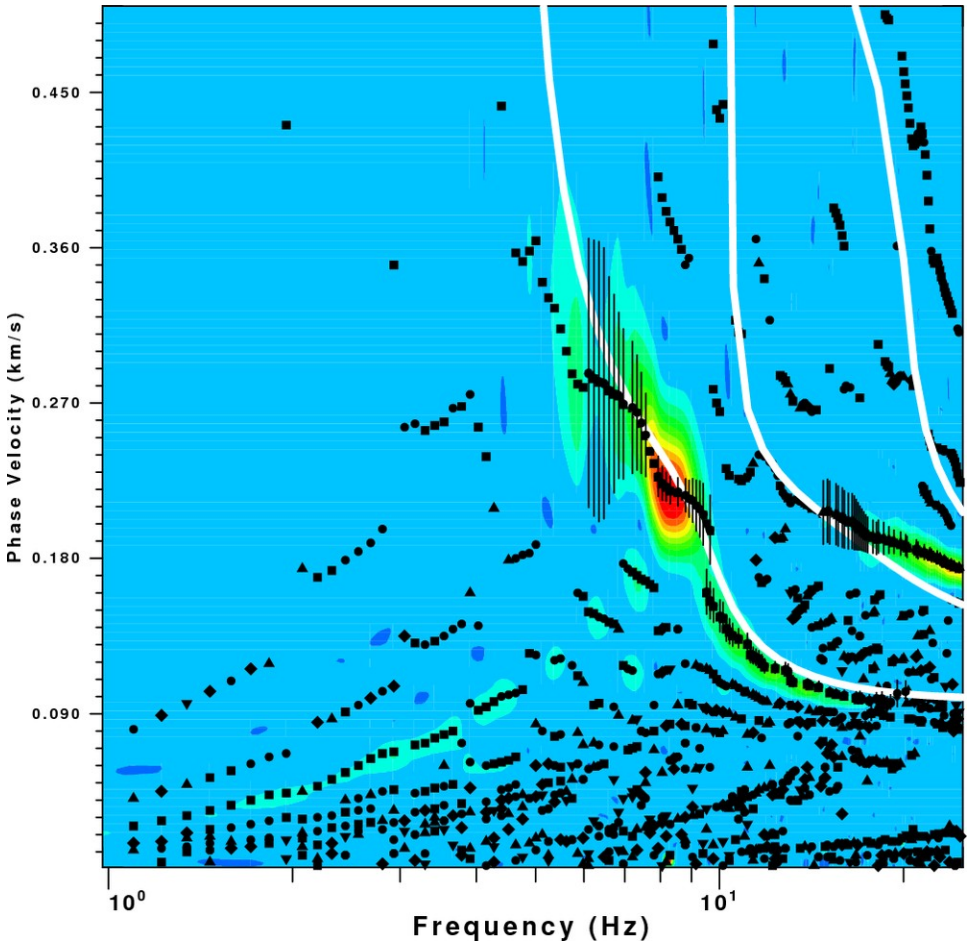


Fig. 3.2. Observed and predicted Rayleigh-wave phase-velocity dispersion for the Riverview site.

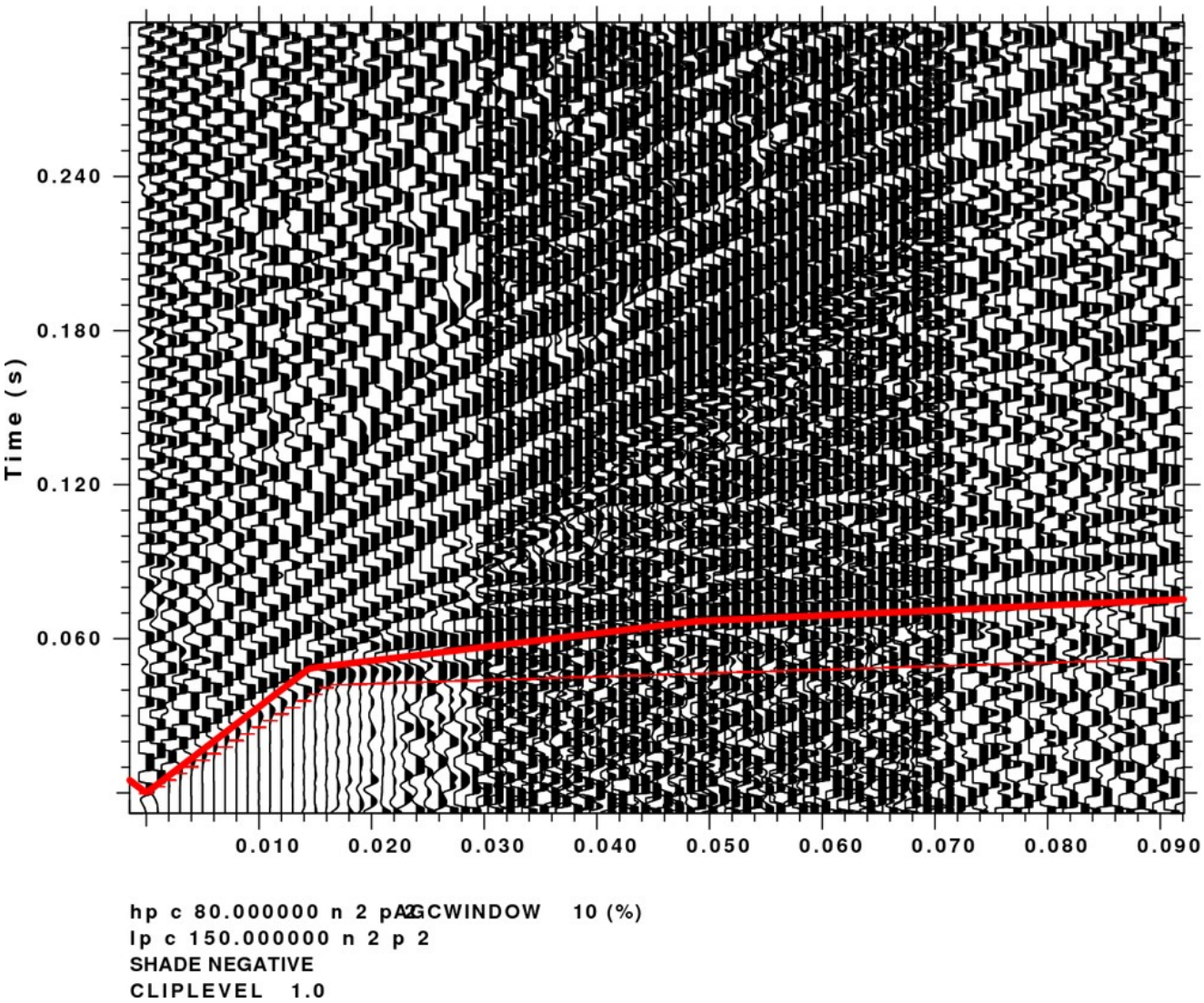


Fig. 3.3. Observed (light red ticks) and predicted (solid red lines) P-wave first arrivals for the Riverview site. The plot annotation indicates the gsac commands used for bandpass filtering the traces. The red curve is the first arrival time prediction based on the model.

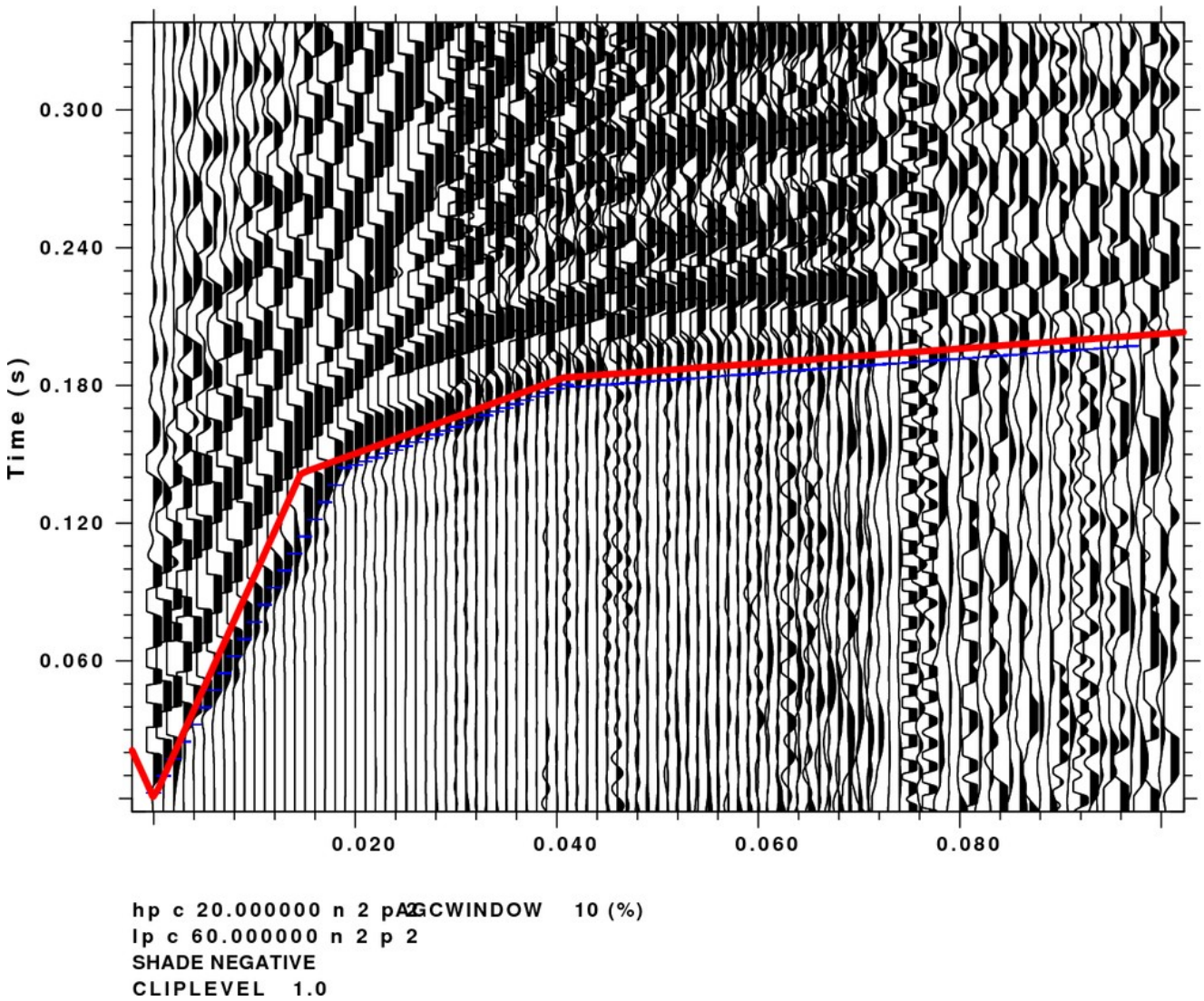


Fig. 3.4. Observed (blue ticks) and predicted (wide red lines) SH-wave first arrivals for the Riverview site. The plot annotation indicates the gsac commands used for bandpass filtering the traces.

### 3.3. Edwardsville Athletic Club:

This data set showed some very nice first arrivals with good signal-to-noise ratios. The model and figures showing the model fits are as follow:

| H(KM) | VP(KM/S) | VS(KM/S) | RHO(GM/CC) |
|---|---|---|---|
| 0.0043 | 0.2401 | 0.1395 | 1.6156 |
| 0.0043 | 0.3781 | 0.2199 | 1.7738 |
| 0.0067 | 1.8170 | 0.2204 | 1.7746 |
| 0.0067 | 1.8170 | 0.2075 | 1.7536 |
| 0.0185 | 2.5750 | 1.6698 | 2.0652 |
| 0.0000 | 4.5169 | 2.5698 | 2.3940 |

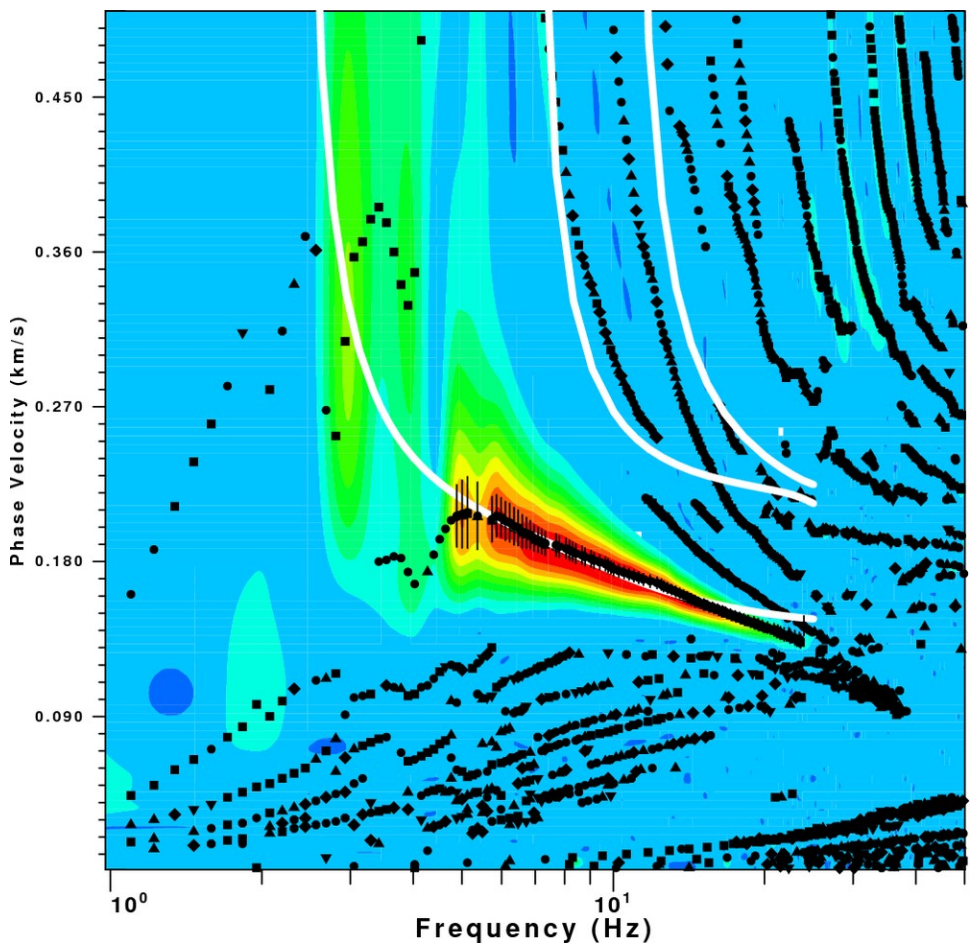


Fig. 3.5. Observed and predicted Love-wave phase-velocity dispersion for the Edwardsville Athletic Club site. The colored contours represent the value of the p_omega(f,c) function, with red being a well defined value. The various points on the plot indicate either other modes or the aliasing inherent in the process. The points with error bars are the phase velocities selected from the contour. The predictions of the fundamental and 1st and 2nd higher modes are given by the solid white curves.

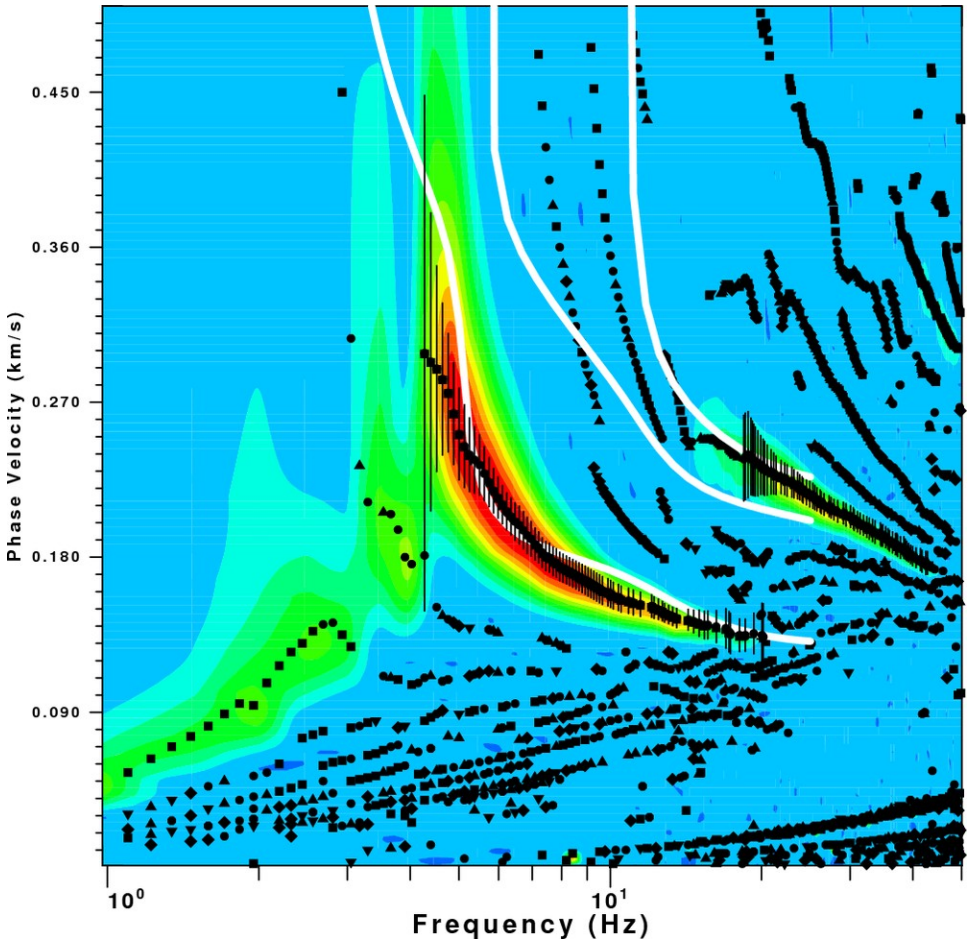


Fig. 3.6. Observed and predicted Rayleigh-wave phase-velocity dispersion for the Riverview site.

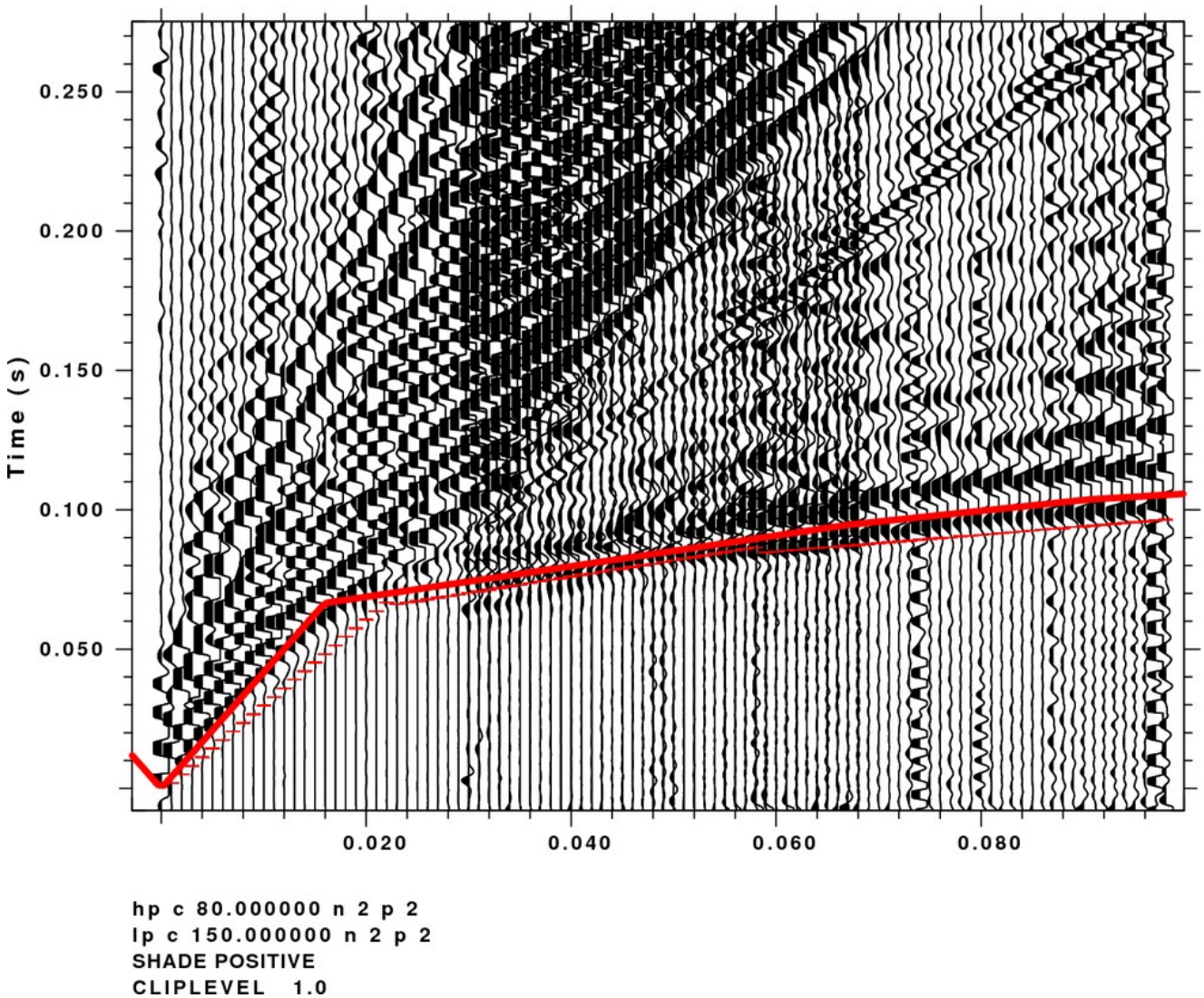


Fig. 3.7. Observed (light red ticks) and predicted (solid red lines) P-wave first arrivals for the Edwardsville Athletic Club site. The plot annotation indicates the gsac commands used for bandpass filtering the traces. The red curve is the first arrival time prediction based on the model.

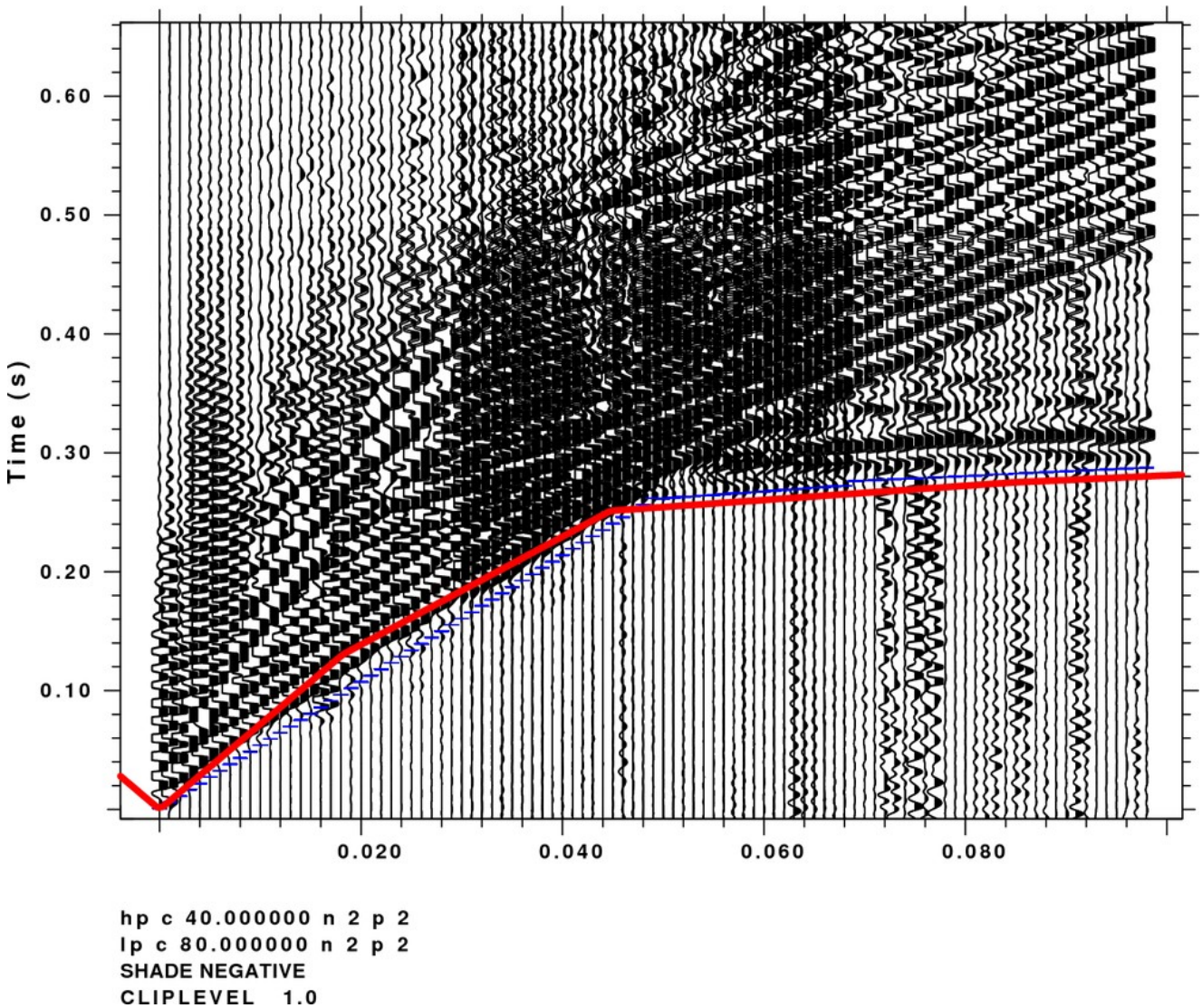


Fig. 3.8. Observed (blue ticks) and predicted (wide red lines) SH-wave first arrivals for the Edwardsville Athletic Club site. The plot annotation indicates the gsac commands used for bandpass filtering the traces. There are reflections in this data set that can be used to constrain the model.

### 3.4. Southern Illinois University Edwardsville

This data set showed some very nice first arrivals with good signal-to-noise ratios. The derived model are the figures showing the model fits are given below:

| H(KM) | VP(KM/S) | VS(KM/S) | RHO(GM/CC) |
|---|---|---|---|
| 0.0019 | 0.2665 | 0.1565 | 1.6555 |
| 0.0068 | 1.5600 | 0.1817 | 1.7076 |
| 0.0021 | 2.1530 | 0.2947 | 1.8755 |
| 0.0135 | 1.8658 | 0.3466 | 1.9319 |
| 0.0135 | 1.8658 | 0.3466 | 1.9319 |
| 0.0000 | 2.1530 | 0.9000 | 2.2634 |

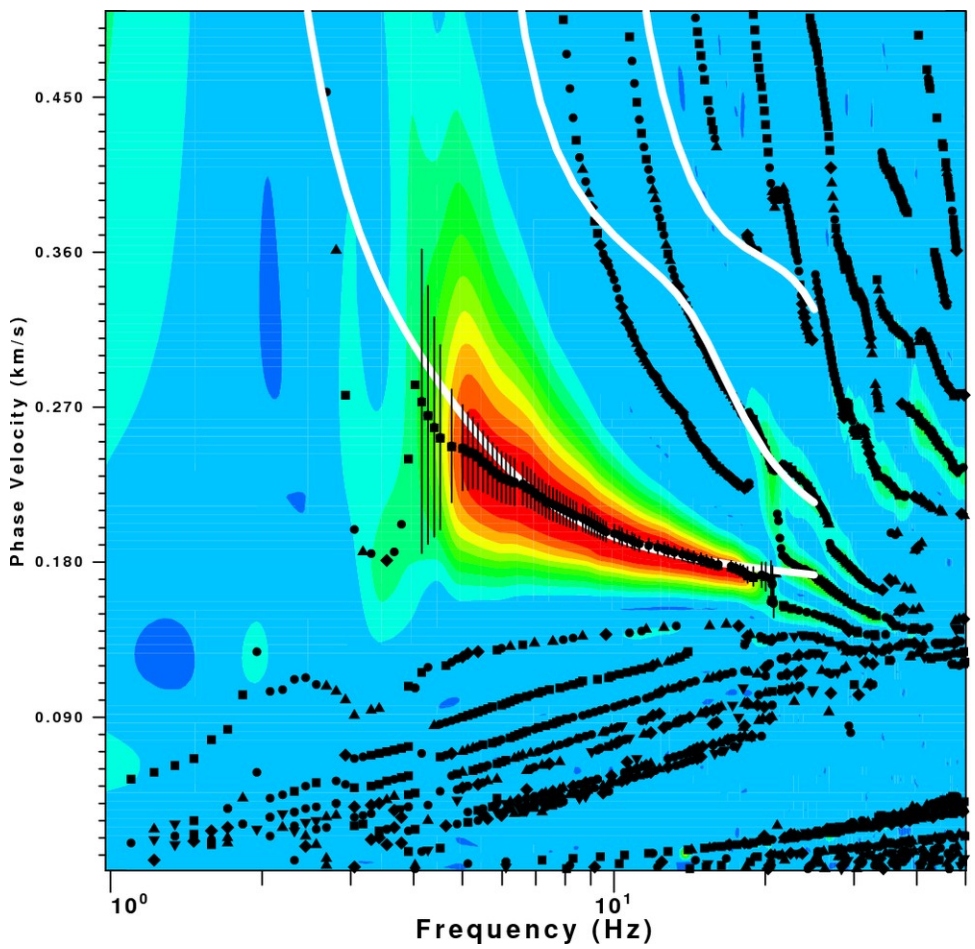


Fig. 3.9. Observed and predicted Love-wave phase-velocity dispersion for the SIUE site. The colored contours represent the value of the p_omega(f,c) function, with red being a well defined value. The various points on the plot indicate either other modes or the aliasing inherent in the process. The points with error bars are the phase velocities selected from the contour. The predictions of the fundamental and 1st and 2nd higher modes are given by the solid white curves.

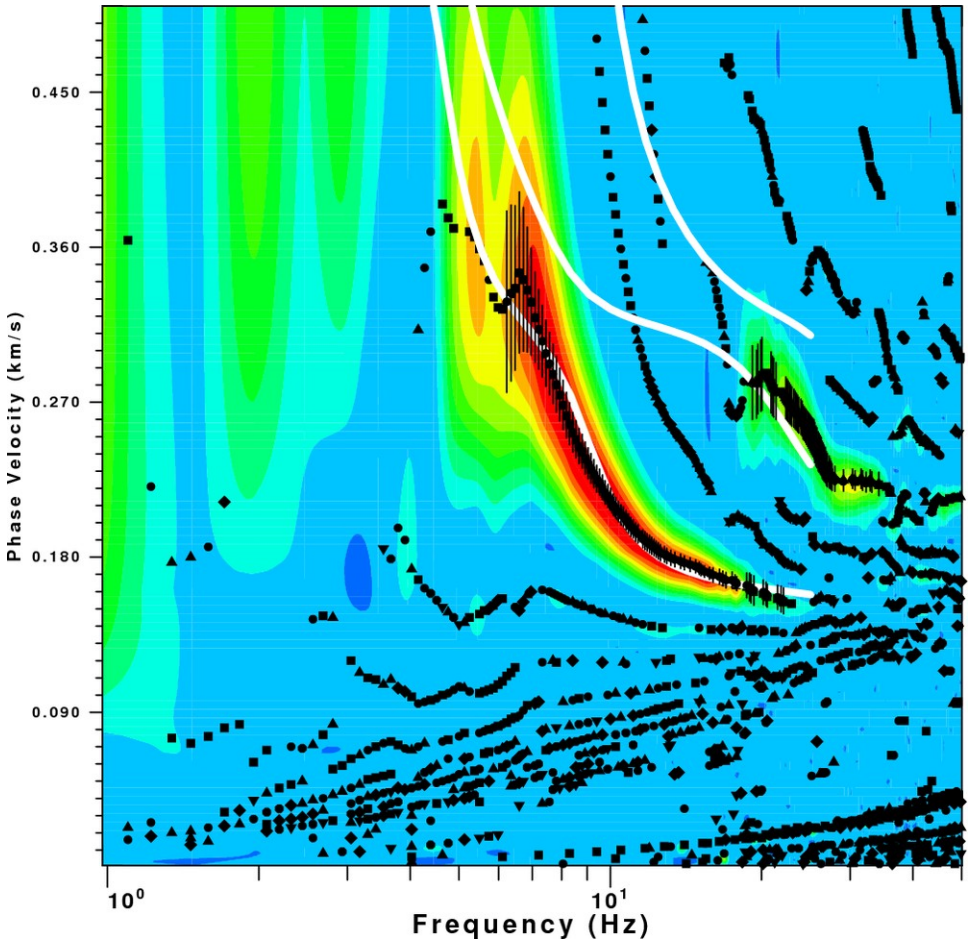


Fig. 3.10. Observed and predicted Rayleigh-wave phase-velocity dispersion for the SIUE site.

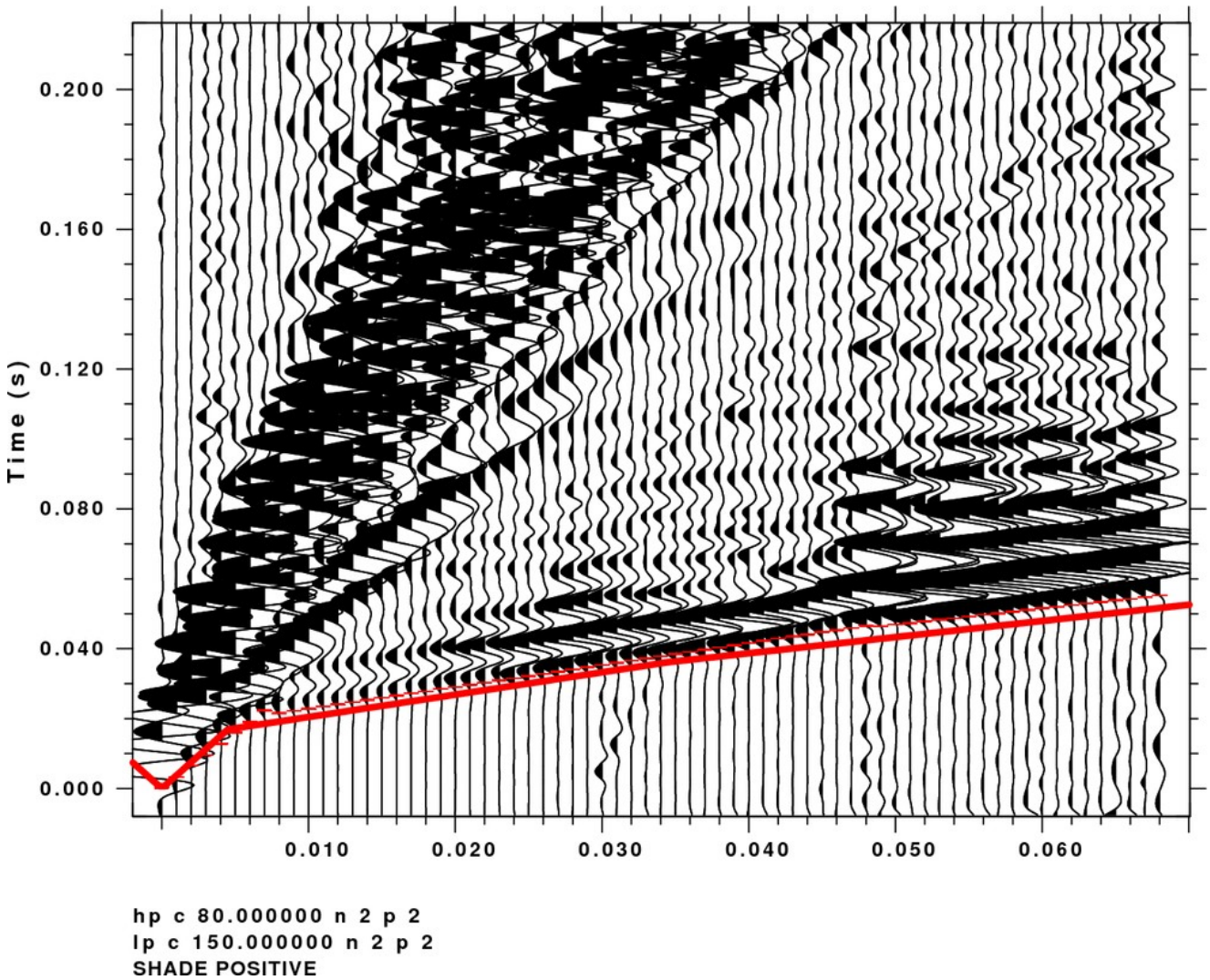


Fig. 3.11. Observed (light red ticks) and predicted (solid red lines) P-wave first arrivals for the SIUE site. The plot annotation indicates the gsac commands used for bandpass filtering the traces. The red curve is the first arrival time prediction based on the model.

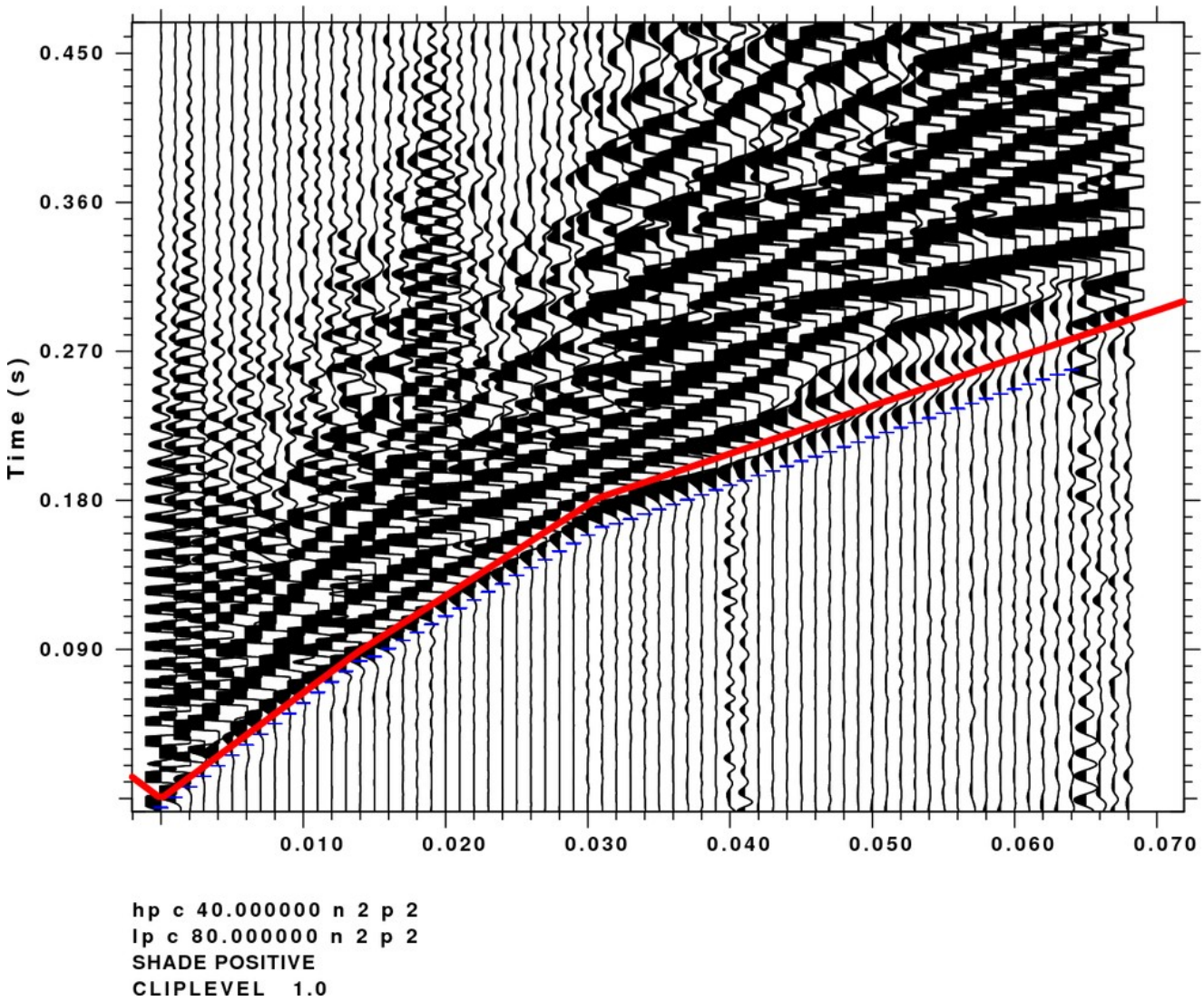


Fig. 3.12. Observed (blue ticks) and predicted (wide red lines) SH-wave first arrivals for the SIUE site. The plot annotation indicates the gsac commands used for bandpass filtering the traces. There is reflection in this data set that can be used to constrain the model.

### 3.5. Jefferson Community College

This data set showed some very nice first arrivals with good signal-to-noise ratios. The derived model are the figures showing the model fits are given below:

| H(KM) | VP(KM/S) | VS(KM/S) | RHO(GM/CC) |
|---|---|---|---|
| 0.0025 | 0.3546 | 0.1861 | 1.7157 |
| 0.0030 | 2.1623 | 1.0812 | 2.3271 |
| 0.0030 | 2.1877 | 1.0938 | 2.3311 |
| 0.0000 | 2.8277 | 1.4138 | 2.4203 |

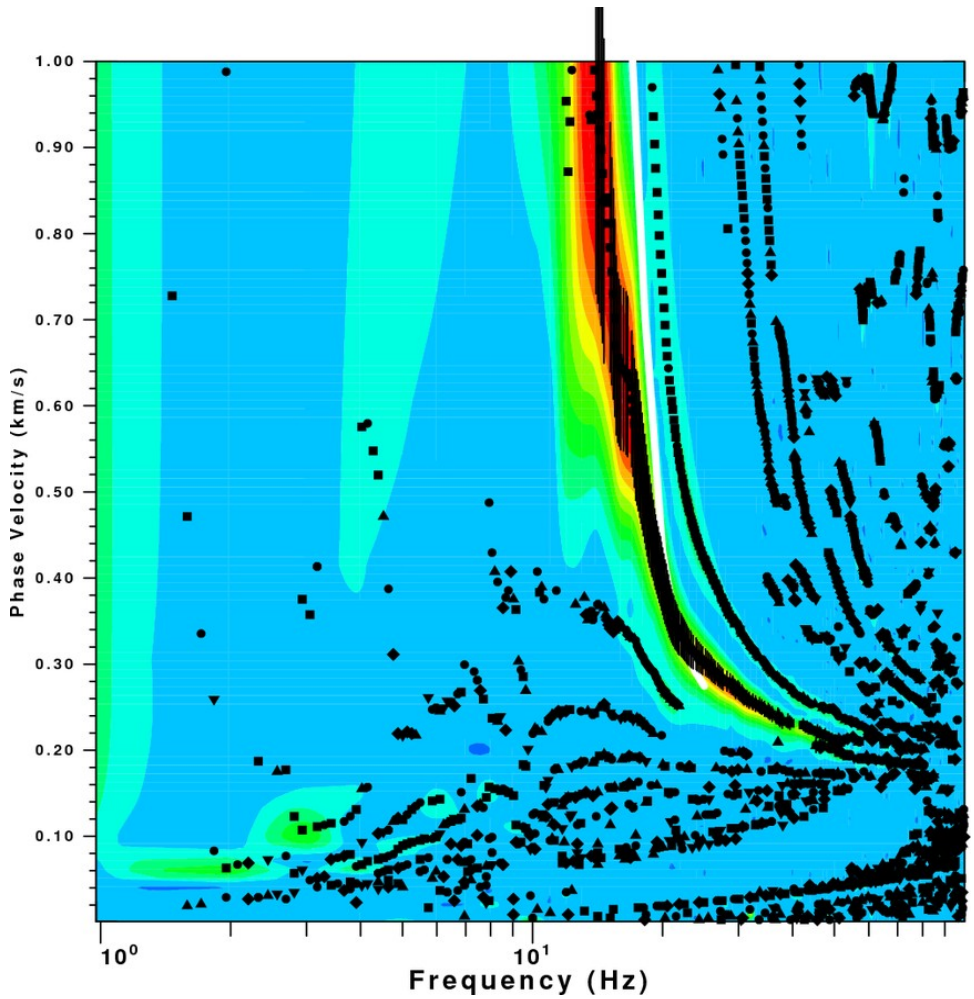


Fig. 3.13. Observed and predicted Love-wave phase-velocity dispersion for the Jefferson Community College site. The colored contours represent the value of the p_omega(f,c) function, with red being a well defined value. The various points on the plot indicate either other modes or the aliasing inherent in the process. The points with error bars are the phase velocities selected from the contour. The predictions of the fundamental mode is given by the solid white curves.

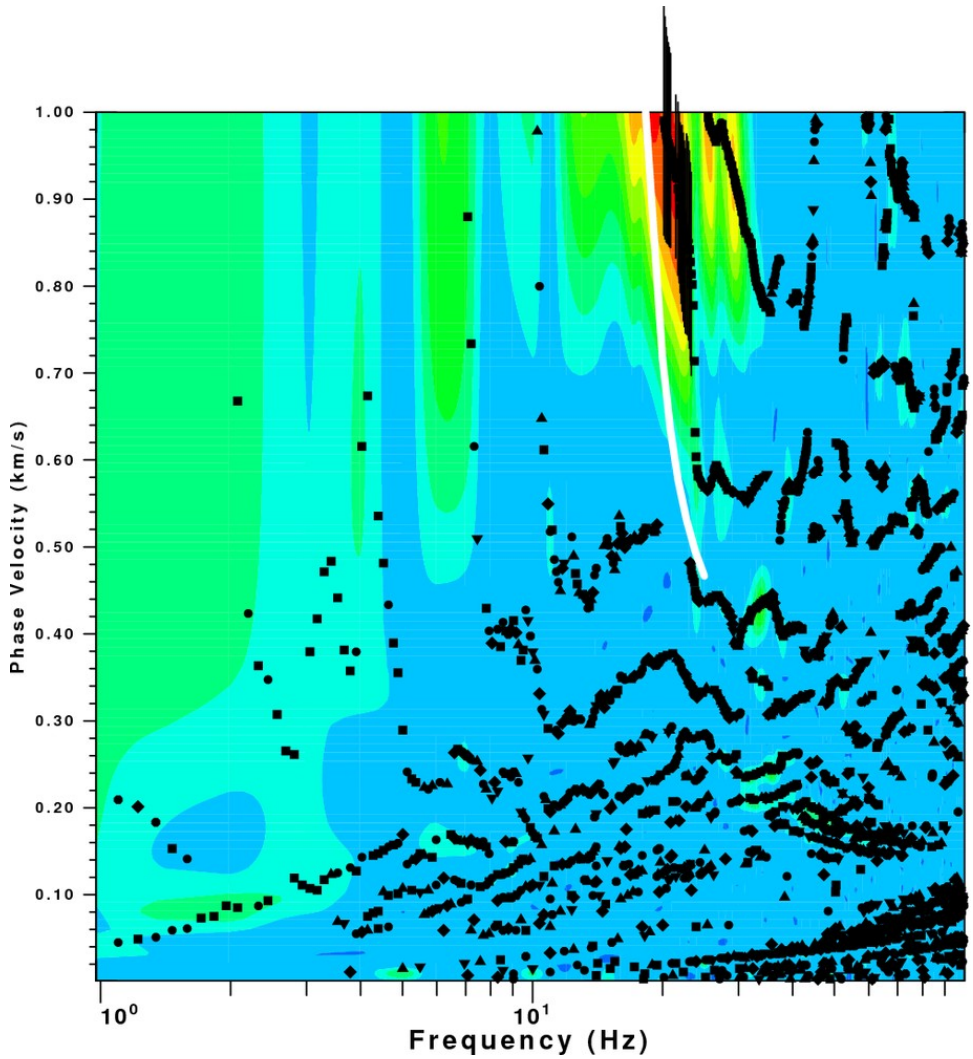


Fig. 3.14. Observed and predicted Rayleigh-wave phase-velocity dispersion for the Jefferson Community College site.

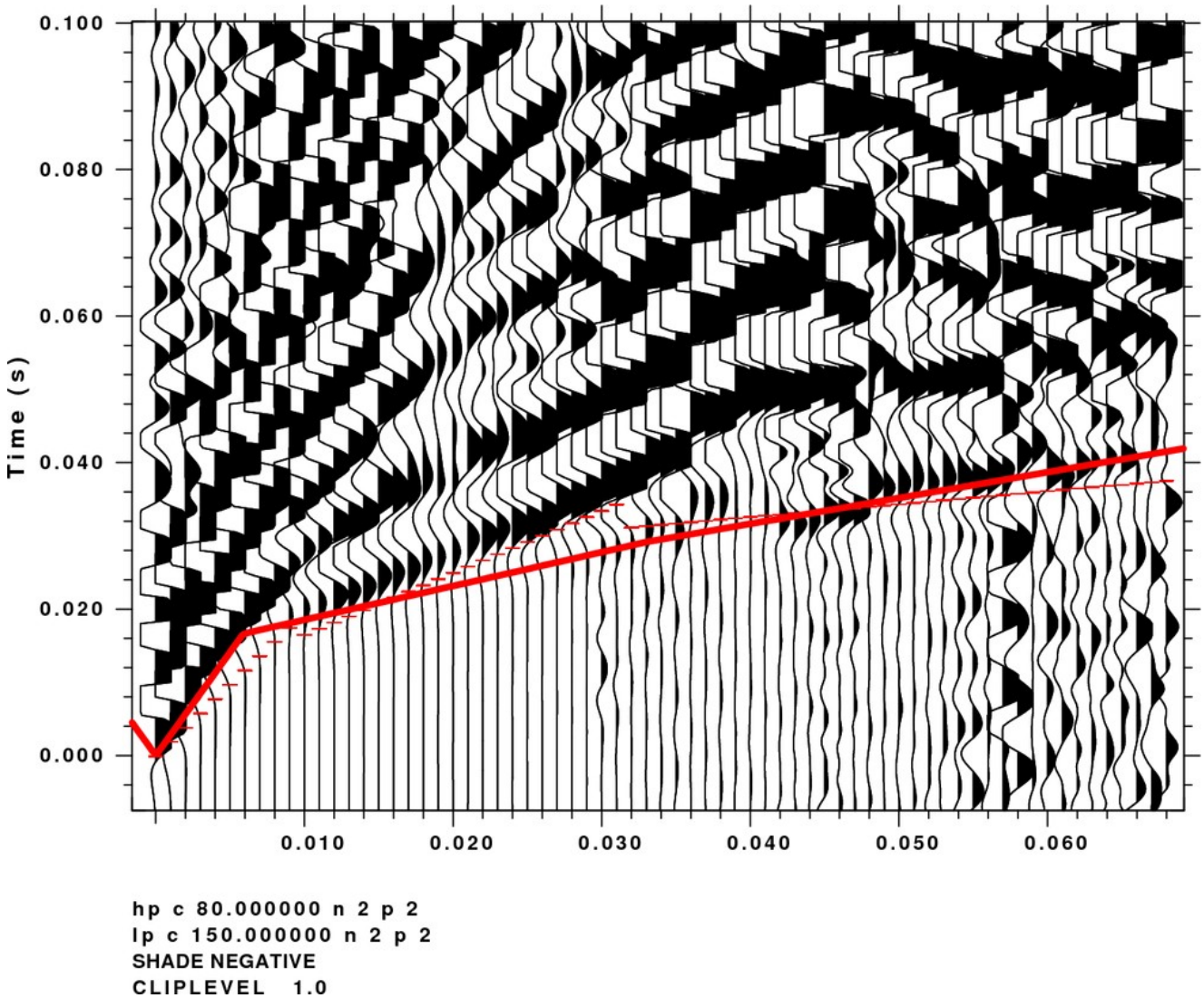


Fig. 3.15. Observed (light red ticks) and predicted (solid red lines) P-wave first arrivals for the Jefferson Community College site. The plot annotation indicates the gsac commands used for bandpass filtering the traces. The red curve is the first arrival time prediction based on the model.

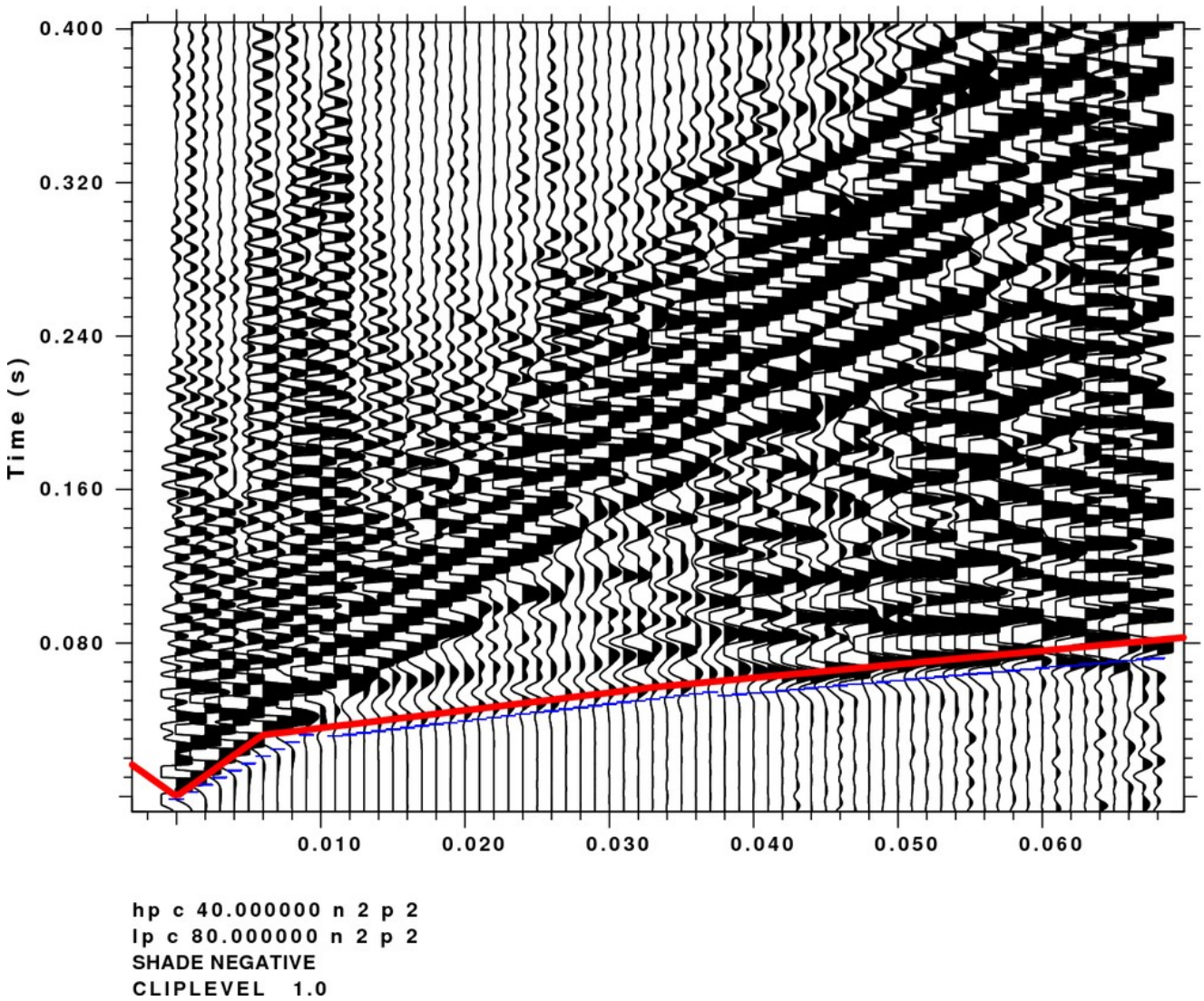


Fig. 3.16. Observed (blue ticks) and predicted (wide red lines) SH-wave first arrivals for the Jefferson Community College site. The plot annotation indicates the gsac commands used for bandpass filtering the traces.

### 3.6. Bellefontaine Park

This data set showed some very nice first arrivals with good signal-to-noise ratios. The derived model are the figures showing the model fits are given below:

| H(KM) | VP(KM/S) | VS(KM/S) | RHO(GM/CC) |
|---|---|---|---|
| 0.0010 | 0.3124 | 0.1191 | 1.5609 |
| 0.0060 | 1.4050 | 0.1230 | 1.5720 |
| 0.0040 | 1.4050 | 0.1467 | 1.6331 |
| 0.0000 | 4.4000 | 2.2000 | 2.3760 |

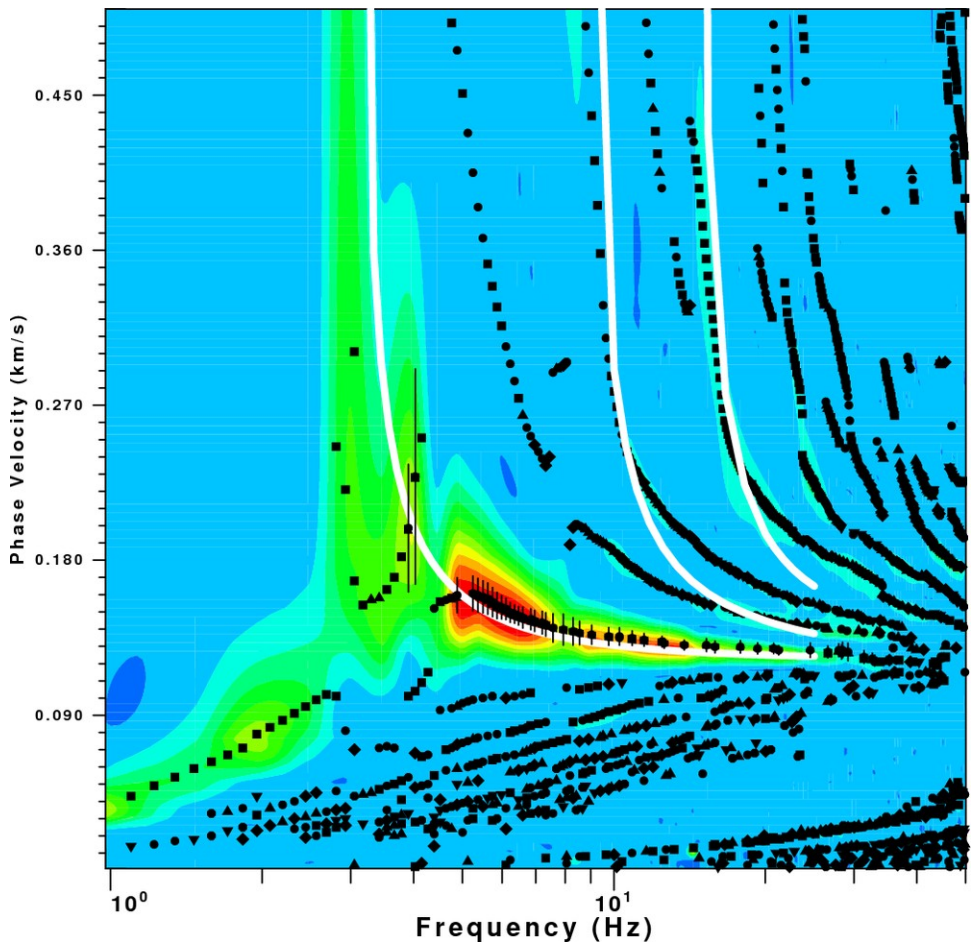


Fig. 3.17. Observed and predicted Love-wave phase-velocity dispersion for the Bellefontaine Park site. The colored contours represent the value of the p_omega(f,c) function, with red being a well defined value. The various points on the plot indicate either other modes or the aliasing inherent in the process. The points with error bars are the phase velocities selected from the contour. The predictions of the fundamental and 1st and 2nd higher modes are given by the solid white curves.

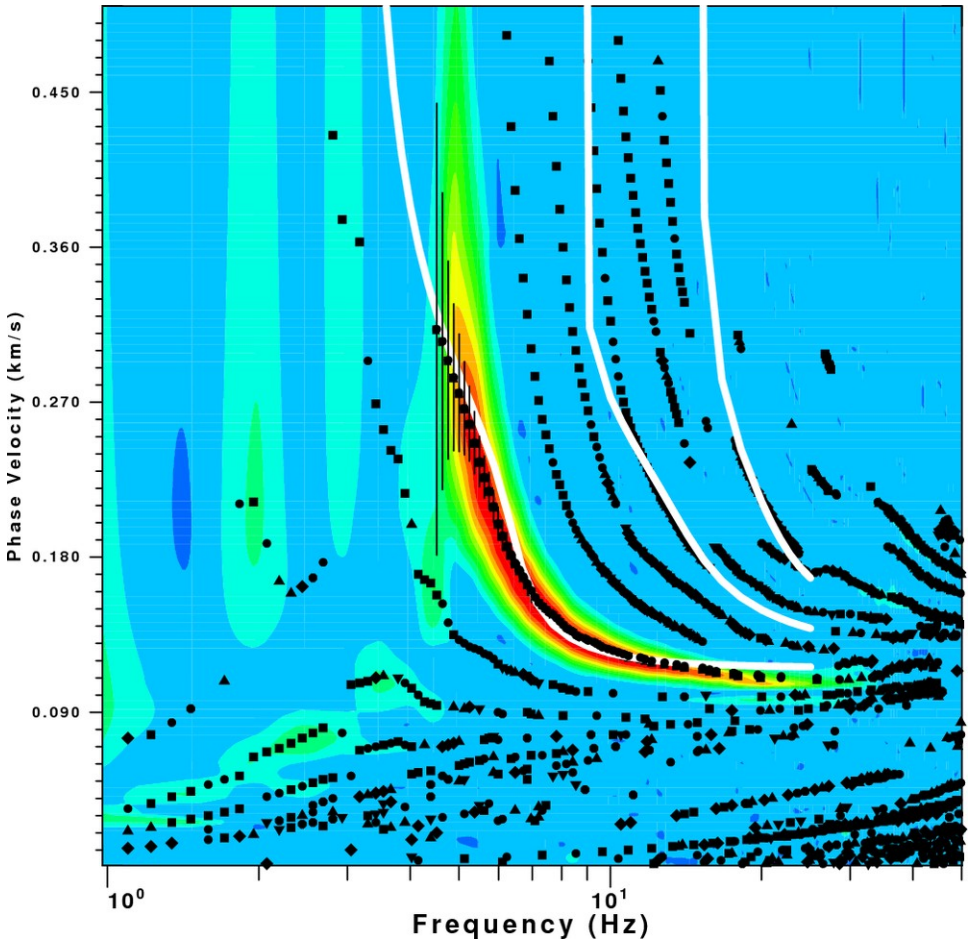


Fig. 3.18. Observed and predicted Rayleigh-wave phase-velocity dispersion for the Bellefontaine Park site.

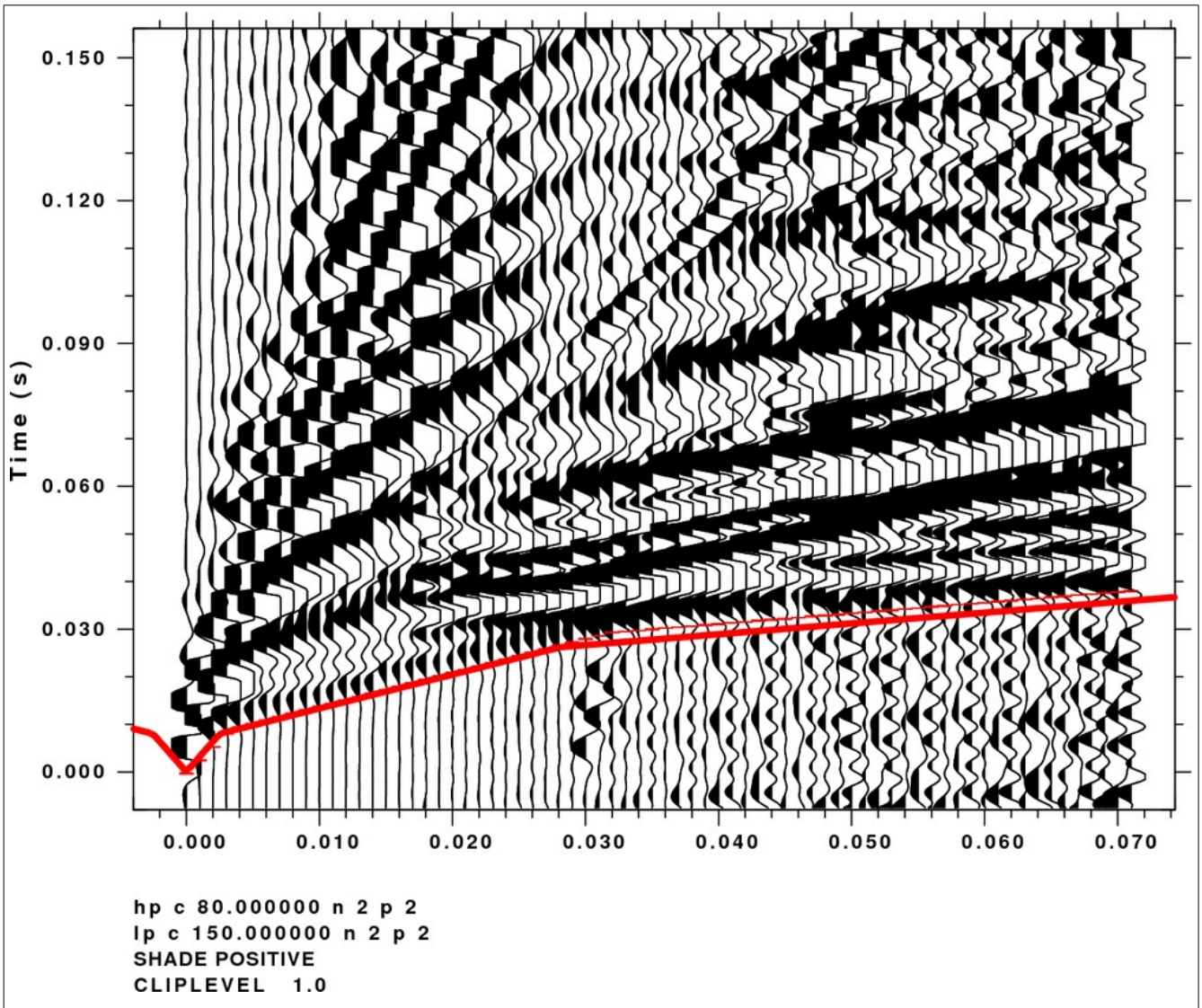


Fig. 3.19. Observed (light red ticks) and predicted (solid red lines) P-wave first arrivals for the Bellefontaine Park site. The plot annotation indicates the gsac commands used for bandpass filtering the traces. The red curve is the first arrival time prediction based on the model.

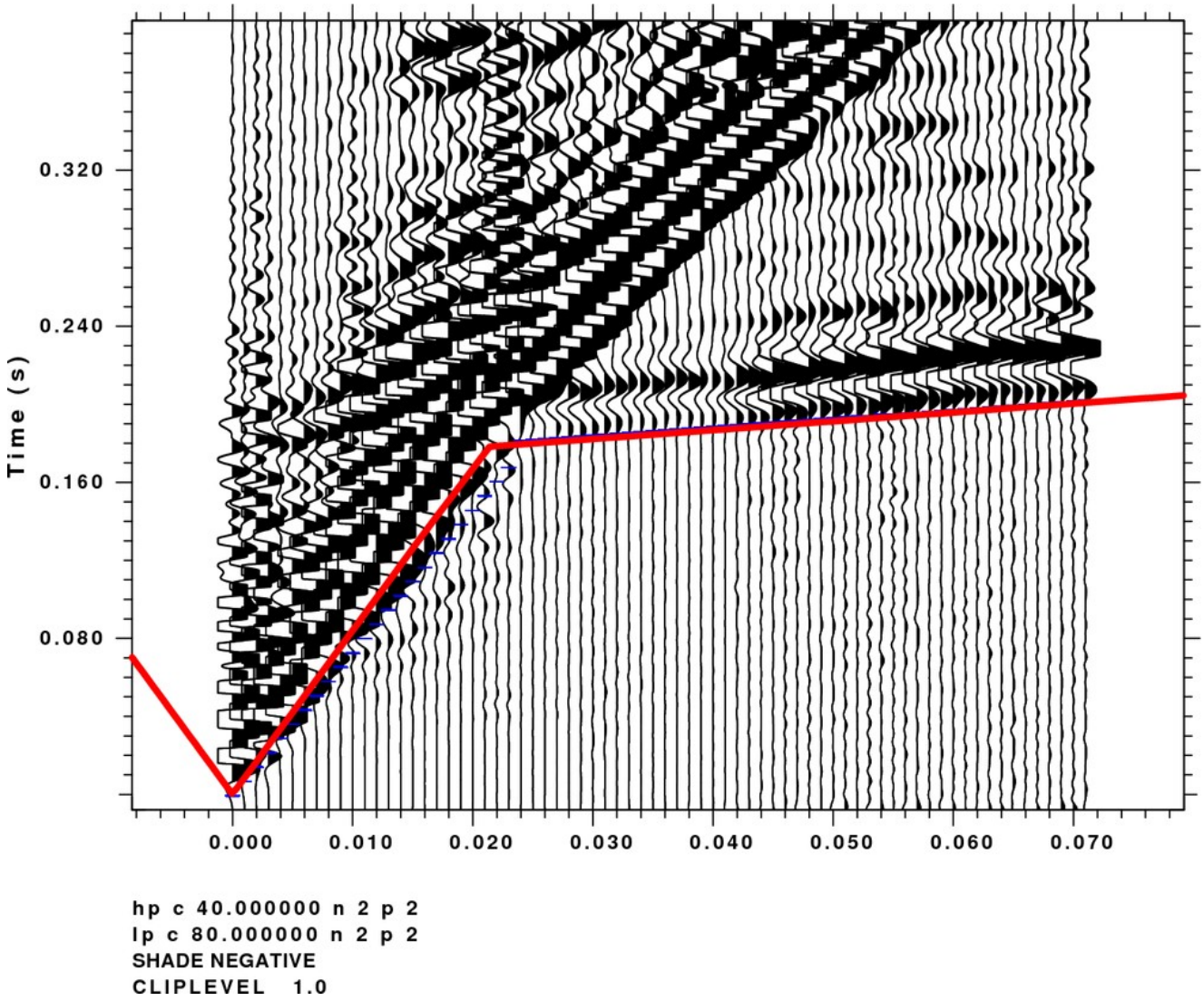


Fig. 3.20. Observed (blue ticks) and predicted (wide red lines) SH-wave first arrivals for the Bellefontaine Park site. The plot annotation indicates the gsac commands used for bandpass filtering the traces. There are reflections in this data set that can be used to constrain the model.

### 3.7. O'Fallon Park

This data set showed some very nice first arrivals with good signal-to-noise ratios. The derived model are the figures showing the model fits are given below:

| H(KM) | VP(KM/S) | VS(KM/S) | RHO(GM/CC) |
|---|---|---|---|
| 0.0030 | 0.4000 | 0.1763 | 1.6970 |
| 0.0020 | 1.6397 | 0.1243 | 1.5755 |
| 0.0120 | 1.6397 | 0.1964 | 1.7345 |
| 0.0000 | 1.6397 | 0.6015 | 2.1234 |

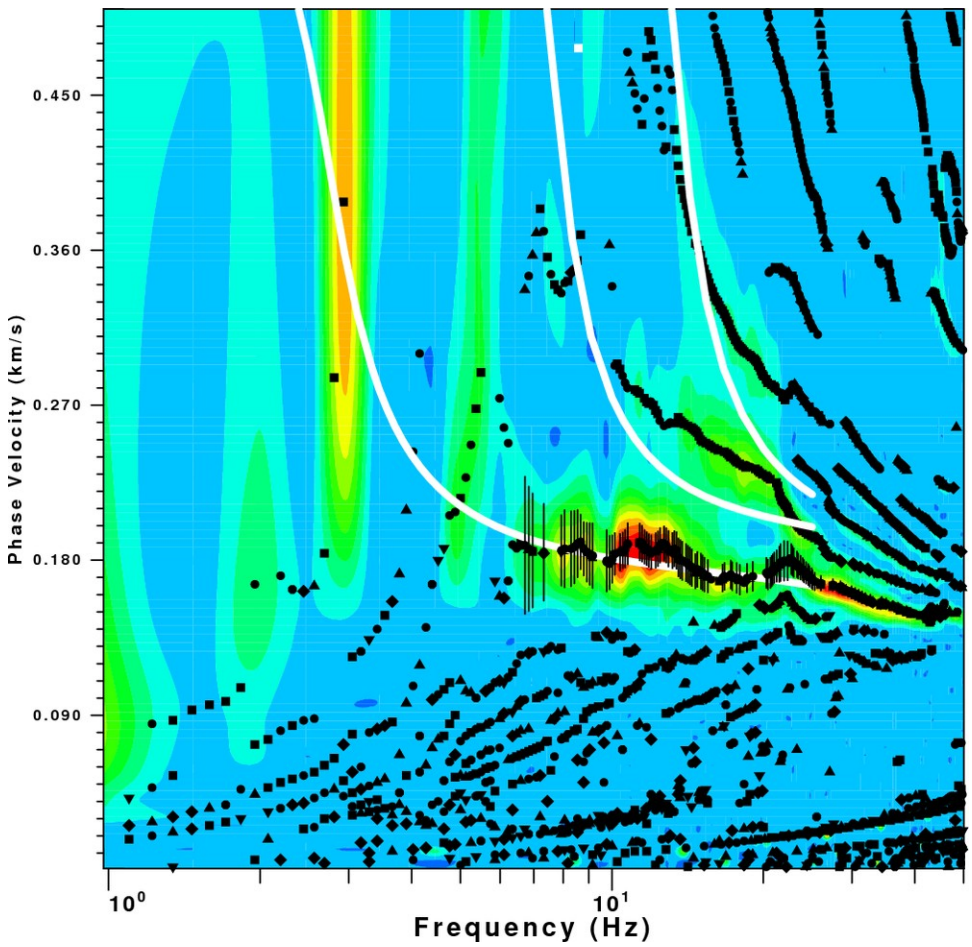


Fig. 3.21. Observed and predicted Love-wave phase-velocity dispersion for the O'Fallon Park site. The colored contours represent the value of the p_omega(f,c) function, with red being a well defined value. The various points on the plot indicate either other modes or the aliasing inherent in the process. The points with error bars are the phase velocities selected from the contour. The predictions of the fundamental and 1st and 2nd higher modes are given by the solid white curves.

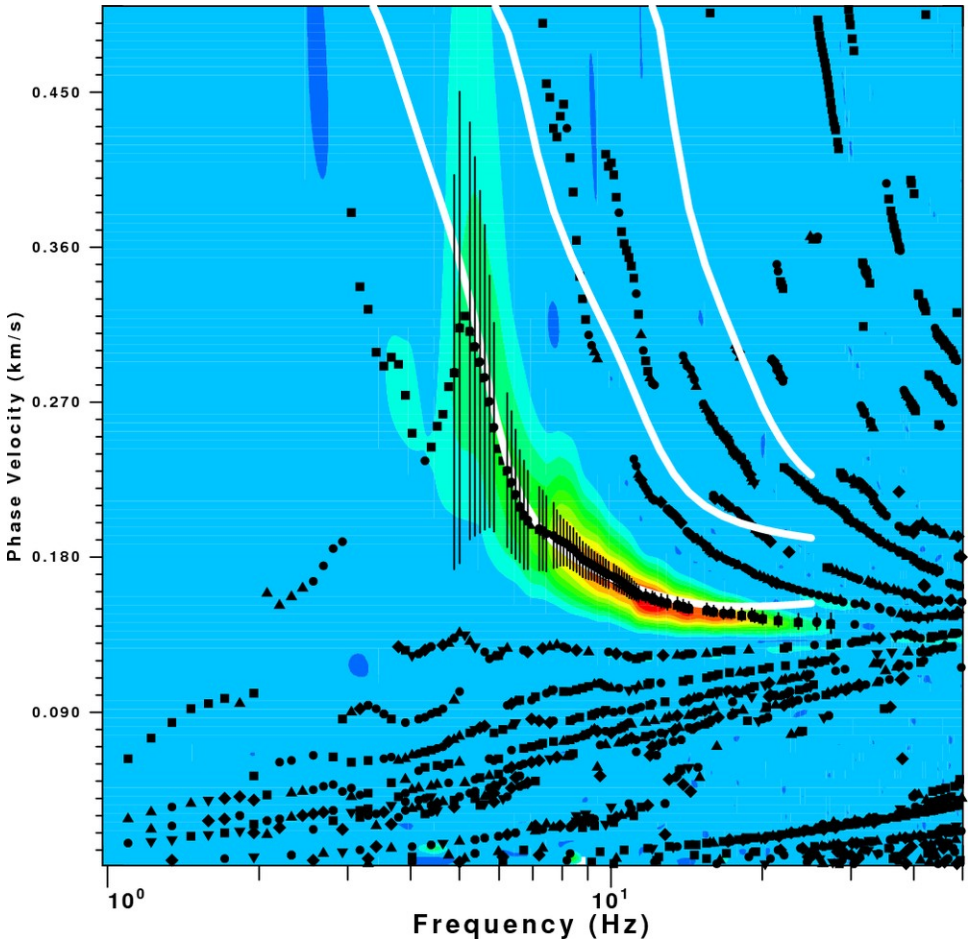


Fig. 3.22. Observed and predicted Rayleigh-wave phase-velocity dispersion for the O'Fallon Park site.

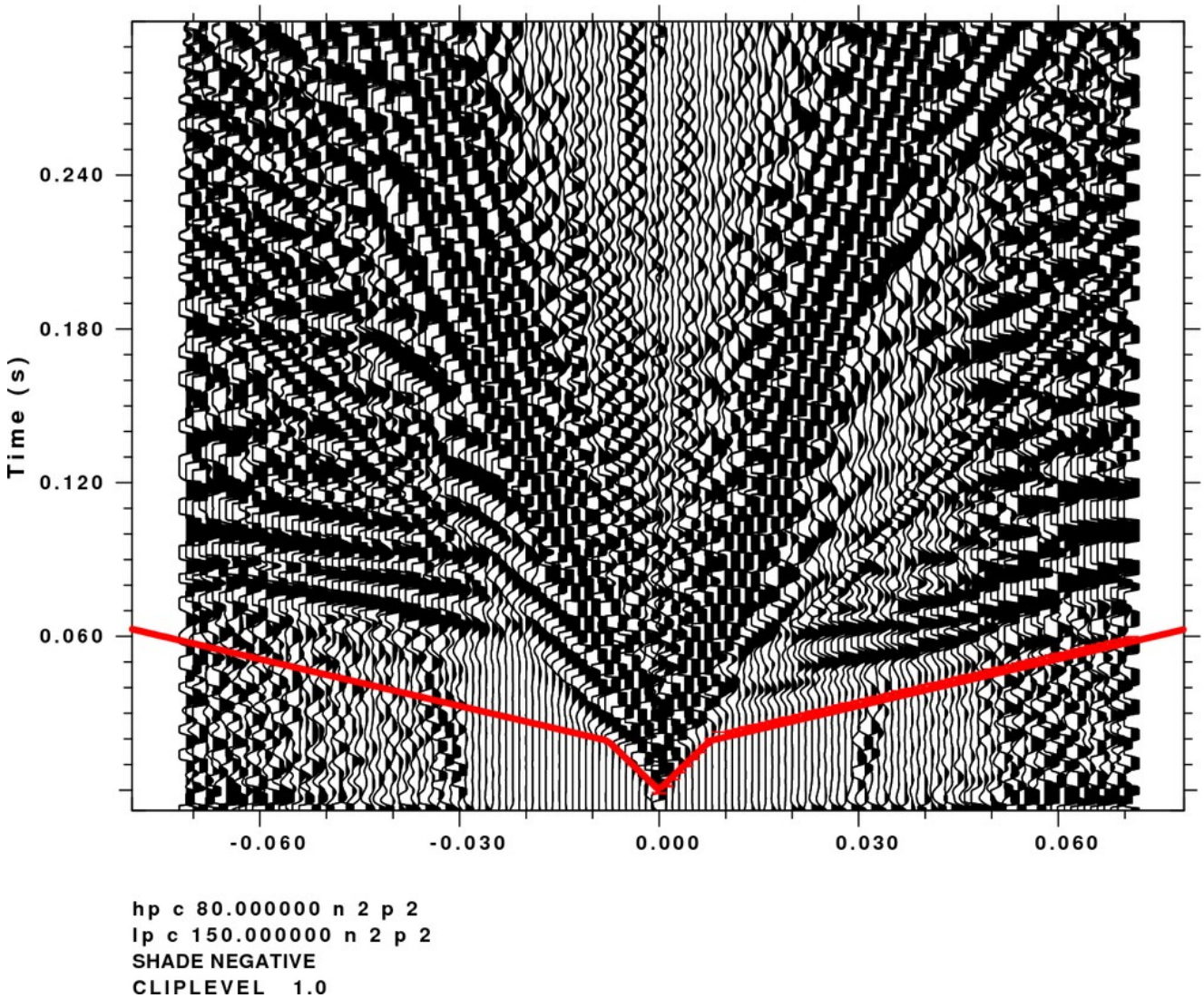


Fig. 3.23. Observed (light red ticks) and predicted (solid red lines) P-wave first arrivals for the O'Fallon Park site. The plot annotation indicates the gsac commands used for bandpass filtering the traces. The red curve is the first arrival time prediction based on the model.

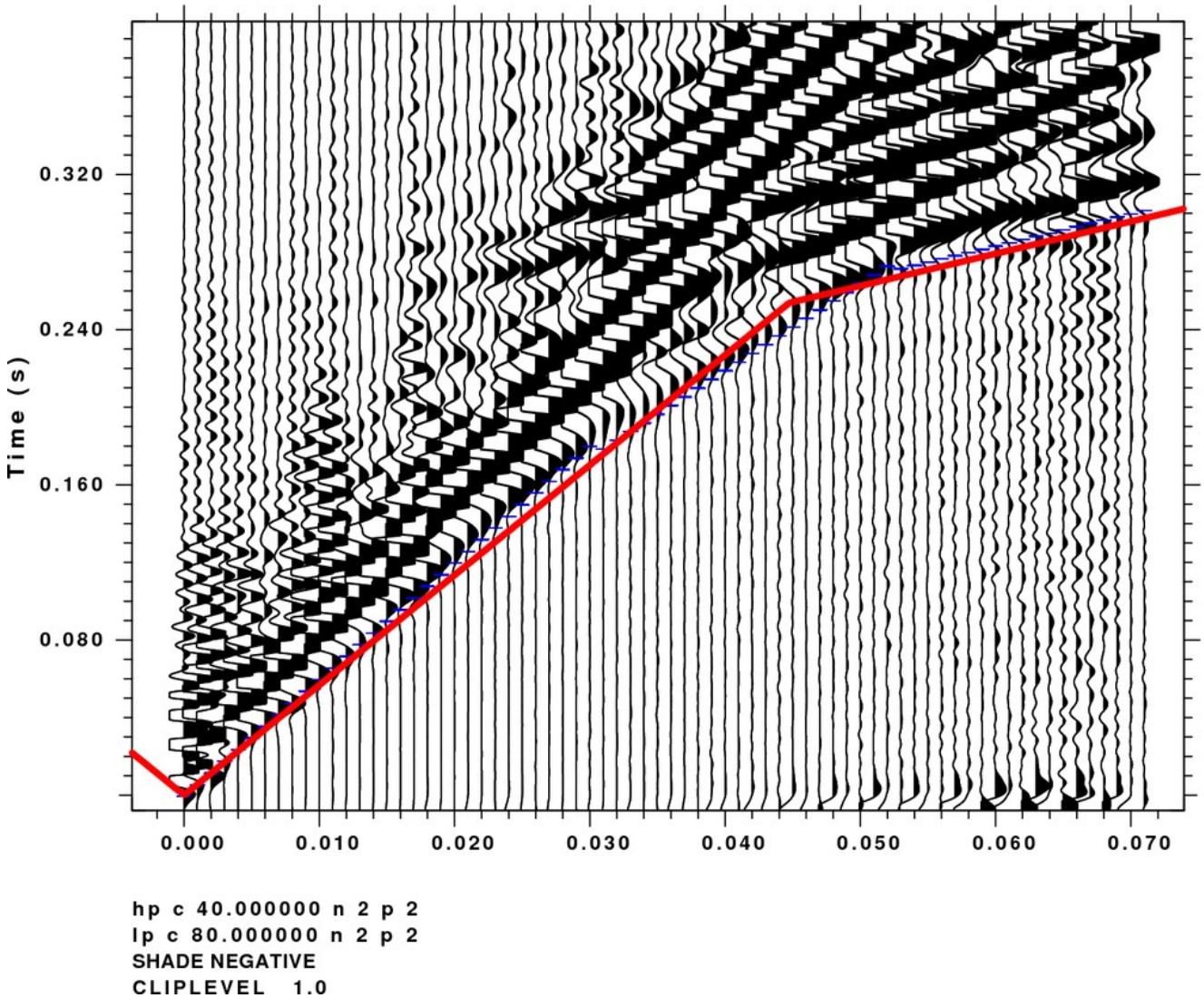


Fig. 3.24. Observed (blue ticks) and predicted (wide red lines) SH-wave first arrivals for the O'Fallon Park site. The plot annotation indicates the gsac commands used for bandpass filtering the traces. There are reflections in this data set that can be used to constrain the model.

### 3.8. Fairground Park

This data set showed some very nice first arrivals with good signal-to-noise ratios. The derived model are the figures showing the model fits are given below:

| H(KM) | VP(KM/S) | VS(KM/S) | RHO(GM/CC) |
|---|---|---|---|
| 0.0050 | 0.4617 | 0.1749 | 1.6942 |
| 0.0050 | 1.6500 | 0.1603 | 1.6641 |
| 0.0050 | 1.6500 | 0.8212 | 2.2316 |
| 0.0050 | 1.6260 | 0.8333 | 2.2366 |
| 0.0000 | 5.0000 | 3.0000 | 2.5000 |

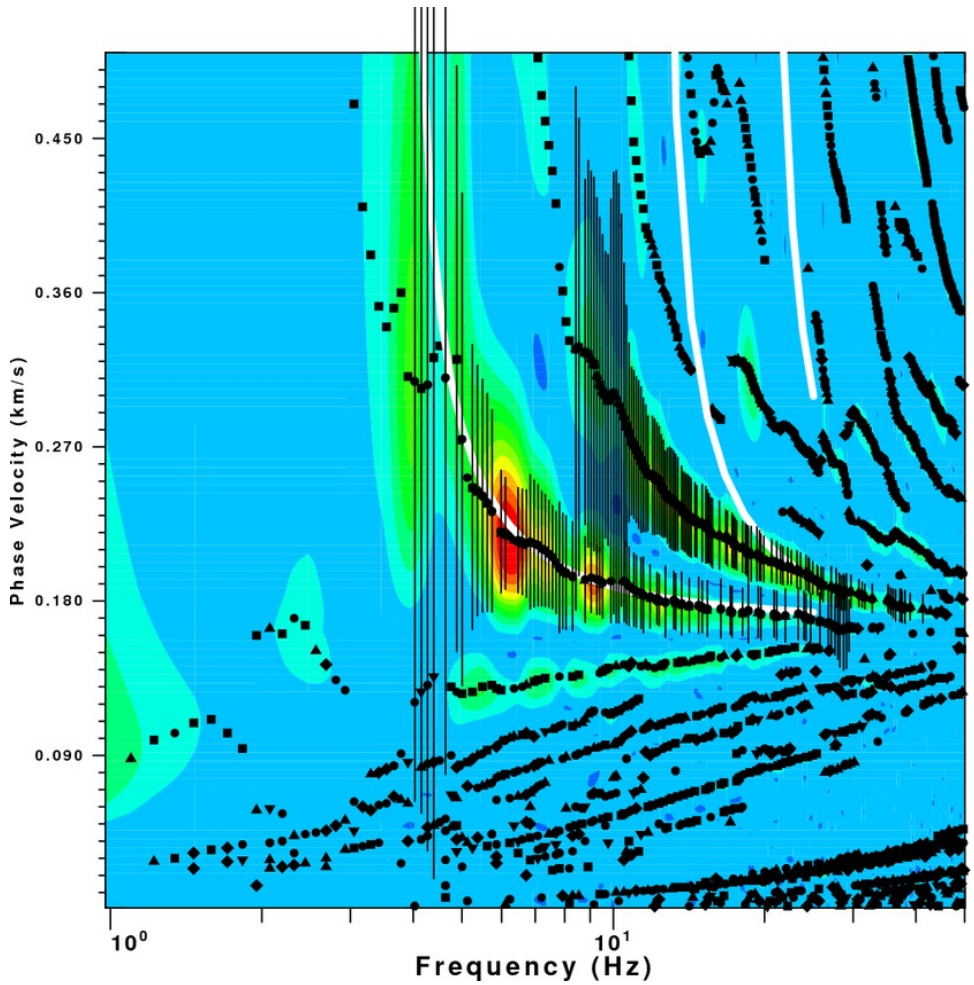


Fig. 3.25. Observed and predicted Love-wave phase-velocity dispersion for the Fairground Park site. The colored contours represent the value of the p_omega(f,c) function, with red being a well defined value. The various points on the plot indicate either other modes or the aliasing inherent in the process. The points with error bars are the phase velocities selected from the contour. The predictions of the fundamental and 1st and 2nd higher modes are given by the solid white curves.

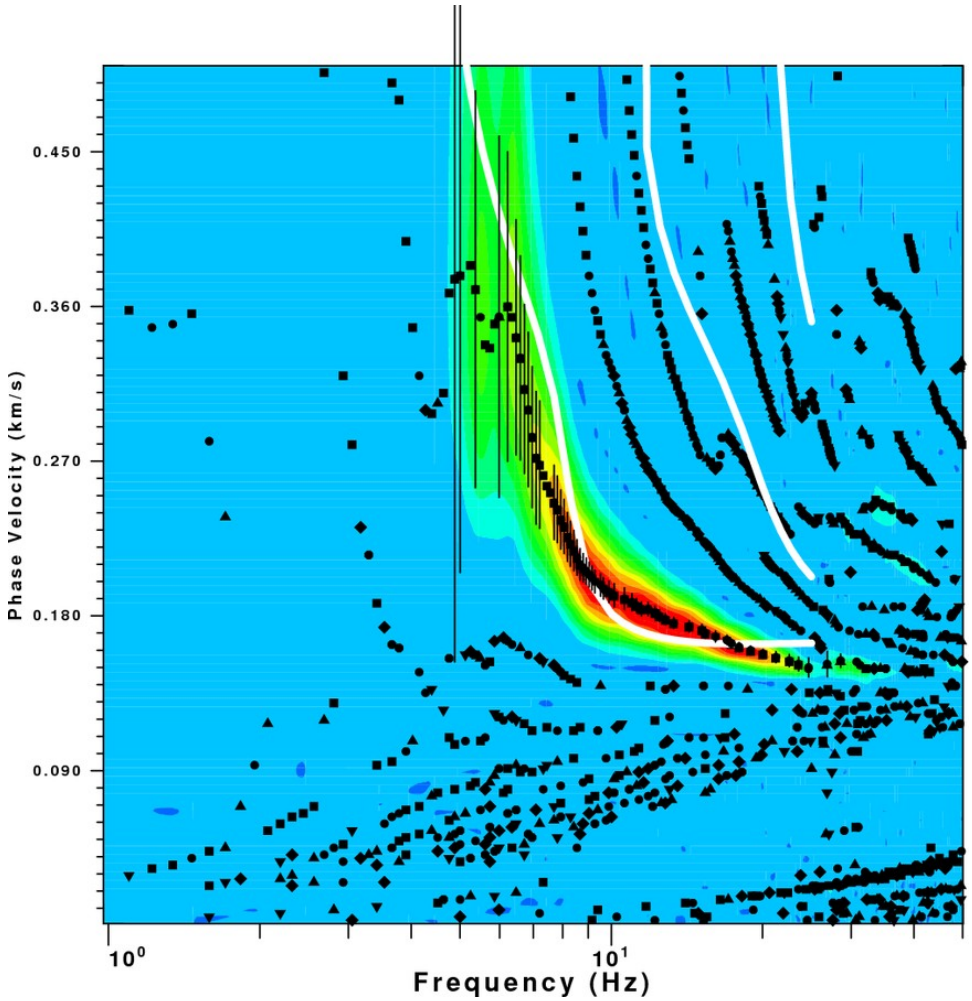


Fig. 3.26. Observed and predicted Rayleigh-wave phase-velocity dispersion for the Fairground Park site.

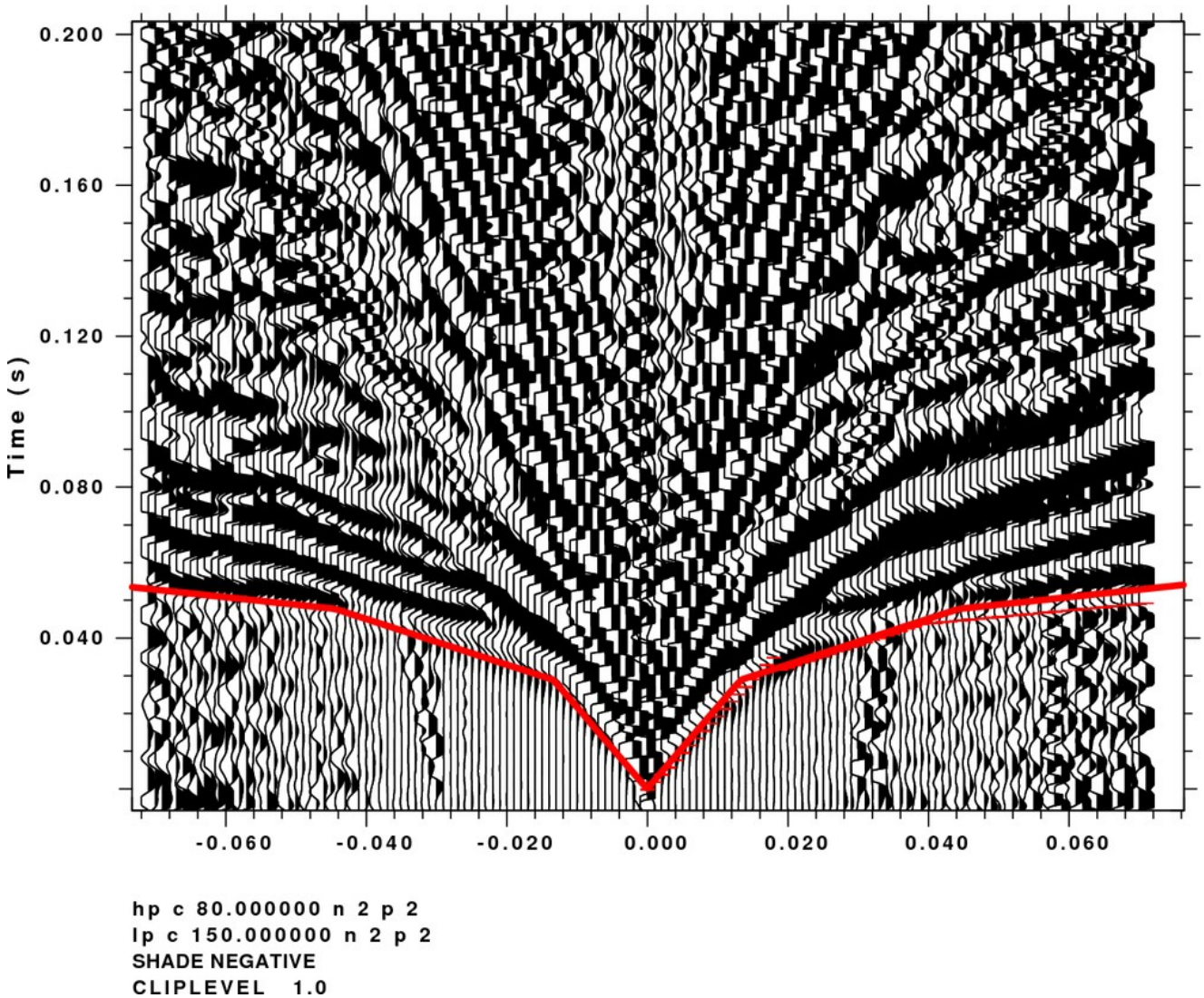


Fig. 3.27. Observed (light red ticks) and predicted (solid red lines) P-wave first arrivals for the Fairground Park site. The plot annotation indicates the gsac commands used for bandpass filtering the traces. The red curve is the first arrival time prediction based on the model.

### 3.9. Other sites

The other sites were not processed because of the poor quality of the data. The Meramec River data set showed very good S reflections. The SLU Soccer field sites needs to be redone.

## 4. Discussion

This effort was successful in the sense that we learned how to perform field experiments consistently. We also noted the differences in data quality. The Jefferson Community College site had the thinnest

soil layer, as evidenced by the high frequencies of the surface-wave dispersion.

The models were initially constructed using the P- and SH-wave first arrivals and then inverting the fundamental model Love- and Rayleigh-wave phase velocity dispersion to adjust the model. There was no subsequent step to refine the model through the use of the first arrival information again.

We have sieved the data sets and now have a good test set for testing the development of a new inversion program that would simultaneously invert both the first arrival times and dispersion. The dispersion output from the *do_pom* procedure yields error bars for each phase velocity point. The error estimate for the first arrival information might just be based on the period of the high pass filter used as part of the processing. A Monte Carlo approach might be used as the basis for such an inversion in order to be able to provide error bounds for the material structure and parameters.

## 5. References

Herrmann, R. B. (2003). Computer programs in Seismology, http://www.eas.slu.edu/People/RBHerrmann/CPS330.html

## Appendix

### 1. Tips for Seismic Refraction Surveys

- Be mindful of the weather. If the ground is saturated with water, you will be unable to obtain energy to the desired distance, especially in an S-Wave survey. Make sure the top layer is dry before doing a survey. Also, beware of sprinkler systems.
- Use the stack mode that saves the most time. If the site is rarely noisy, keep the seismograph on autostack. You can still unstack and delete noisy shots. If noise sporadically arises, use the preview mode so that you can reject noisy shots.
- Planting the phones is very important. If the sensors are not perpendicular to the path of the waves they are measuring, extra noise will be present throughout the trace. Double check that the phones are planted and functioning properly before completing a survey.
- The display screen on the recorder is very difficult to see and read in the sun. If possible, use an umbrella or place the recorder in the shade.
- Record the gps coordinates of both ends of the line. This eliminates the necessity of having a bearing.
- Nearby traffic and construction sites will create noise in the traces. Always keep this in mind.
- The contacts on the geophone cables and the contacts on the geophones themselves should be kept as clean as possible. Remove dirt with a rag and water, but use an appropriate cleaning solution for other unwanted residue.
- Learn the menus and other options on the seismograph before doing any type of fieldwork.
- If possible, do not complete a noise test with an overbearing source of noise in the area. Wait for it to leave or at least get far enough away.
- Gloves and earplugs are a good idea when swinging the hammer.
- Put as little stress and strain on the shot line as possible. Give yourself more than enough slack. Roll the cables as tightly as possible so that any kinks that develop during the fieldwork do not become more permanent than they have to be.
- Choose a reasonably flat spot to complete the survey. The flatter a spot is, the better. Bumps and dips in the ground will make your interpretation less accurate.